

Advanced Trajectory Tracking for UAVs Using Combined Feedforward/Feedback Control Design

Mohamed Kara-Mohamed¹

¹ School of Engineering and The Built Environment,
Birmingham City University, Birmingham, B4 7XG, UK.

Mohamed.Kara-Mohamed@bcu.ac.uk

Abstract

Trajectory tracking is a major challenge for UAVs. The more complex the trajectory is, the more accurate tracking is required with minimum divergence from the trajectory. Apart from active trajectory tracking mechanisms, current solutions to accurate trajectory tracking in narrow areas require low speed motions. This paper presents a systematic design methodology using centralised feedforward/feedback control architecture for advanced trajectory tracking without compromising the speed of the vehicle. Using the H_∞ norm as a measure for the design criteria, the proposed method proves fast tracking with no overshooting and less actuators energy compared with single degree-of-freedom feedback control method. The results are verified using simulations for two systems: a tri-rotor VTOL UAV (fully actuated system), and a quadrotor trainer (over-actuated system).

I. INTRODUCTION

Unmanned Aerial Vehicles (UAVs) have seen significant growth with expanding employment in various sectors [1], [2]. Generally speaking, two main advantages can be highlighted for the use of UAVs compared with manned vehicles; they are less costly and have no risk on pilot's life [3]. UAVs were introduced during World War I for pure military tasks, and since then, they have been developing for wide range of applications [4]. Recently, on the top of their integration in military services for collecting data, observing enemies or even lethal attacks ([5], [6] and references therein), UAV systems have been used in civil missions of wide spectrum [7], [8], [9]. For instance, in the field of scientific research, UAVs are used for investigating areas, collecting data, watching volcanoes, forecasting weather, monitoring isolated territories and other various activities [10], [11], [12]. This wide range of applications has raised research interest in UAVs and made the field of UAV design and operation the most dynamic developing sector in aerospace industry [13], [4].

The problem of trajectory tracking is one of the major challenges for UAV guidance and control. Conventionally, this problem is formulated using tracking-error correction methods associated with Lyapunov stability-based control design [14], [15], [16]. However, finding the suitable candidate for Lyapunov function is challenging specially for complex nonlinear systems. For uncertain or disturbed trajectories, stochastic based methods [17] and nest saturation [18] are examples of existing design methods in literature to enhance the trajectory tracking performance. Methods like dynamic inversion [19], nonlinear

control [20], sliding mode [21] and model predictive control [22] exist also in literature. However, these control techniques are complex in implementation and suffer from certain limitations related to the feedback loop and model accuracy [23]. Active trajectory tracking methods, which are mainly vision-based systems, are proposed in literature as alternatives for enhanced trajectory tracking [24]. Nevertheless, vision-based tracking is computationally expensive and requires certain on-board processing capacities which is not always available specially for miniature air vehicles (MAVs).

This paper concerns the problem of trajectory tracking for narrow certain areas, where the vehicle has to follow its trajectory with minimum overshooting and errors. Complex industrial sites are ideal examples of such a scenario where the UAV needs to follow its trajectory in narrow spaces. Wide divergence from trajectory could result in crashing and multi damage to the vehicle and surroundings. The available solution to this problem is to decrease the bandwidth of the system and slow the speed of the vehicle. However, this affects the efficiency of the UAV and increases the timing cost of the service. In this paper, we develop a special form of two degree-of-freedom feedforward/feedback (Ff/Fb) control architecture to stabilise the vehicle and at the same time guarantee good trajectory tracking without decreasing the bandwidth of the system. This is the first article in the field to investigate this control method for UAV applications. The results are demonstrated via simulation by using two examples. The first example is for a complex fully actuated tri-rotor UAV and the second example is for an over-actuated quadrotor trainer. The proposed control system shows superiority over robust feedback-only control. The performance is measured using the \mathcal{H}_∞ norm of the closed loop transfer functions.

In Section II, the proposed Ff/Fb structure is discussed in detail. The simulation examples are investigated in Section III and Section IV, followed by conclusion in Section V.

II. CONTROL SYSTEM DESIGN

Consider the system in Figure 1. The diagram is a representation of the architecture proposed in [25] which in turn builds on [26], [27]. Let P be the linearised system of the nonlinear UAV model that is linearised via any linearisation method. The linearised system P can be factorised over \mathcal{RH}_∞ such as $P = NM^{-1}$ where N and M are coprime factors. Further details on coprime factorisation can be found in [26].

The control objectives considered in this paper are to stabilise the UAV and ensure good trajectory tracking with good speed, no divergence and less input power. These design objectives can be stated in terms of the transfer function matrix $T = \begin{bmatrix} T_{ry} \\ T_{ru} \end{bmatrix}$ where T_{ry} is the trajectory tracking transfer function from the reference vector r to the output vector y and T_{ru} is the control effort transfer function from the reference r to the control input u . From Figure 1, we have:

$$T = \begin{bmatrix} (I + PC)^{-1}P(CY + X) \\ (I + CP)^{-1}(CY + X) \end{bmatrix} \quad (1)$$

From the properties of Woodbury matrix identity [28] and for matrices A, B, U and V of suitable dimensions, we have:

$$(A - UB V)^{-1}UB = A^{-1}U(B - VAU)^{-1} \quad (2)$$

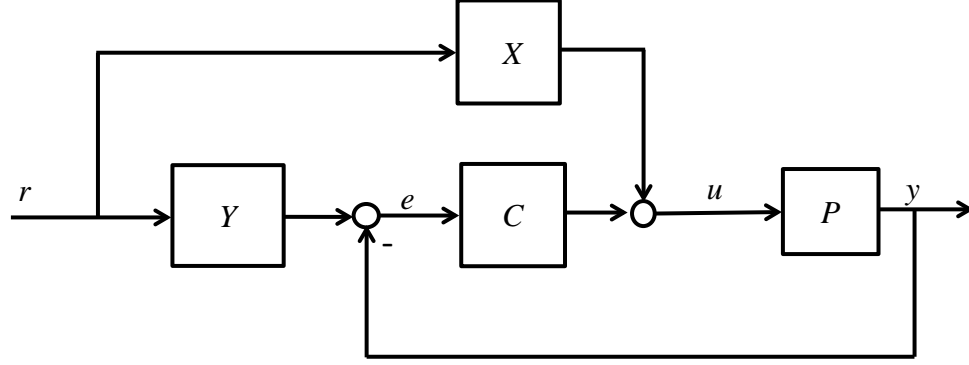


Figure 1. Combined Ff/Fb control to enhance UAV's trajectory tracking.

Assuming that $A = I$ and $B = I$ gives $(I - UV)^{-1}U = U(I - VU)^{-1}$.

For the case in hand, substituting $U = -P$ and $V = C$ enables us to write $(I + PC)^{-1}P = P(I + CP)^{-1}$. Therefore, T can be written as:

$$T = \begin{bmatrix} P \\ I \end{bmatrix} (I + CP)^{-1} (CY + X) \quad (3)$$

Now, let the filters X and Y be designed using the coprime factors of the linearised system such that $X = M$ and $Y = N$. Given that $P = NM^{-1}$, this makes the resulting transfer function matrix T as:

$$T_{\text{Ff/Fb}} = \begin{bmatrix} NM^{-1} \\ I \end{bmatrix} (I + CNM^{-1})^{-1} (CN + M) \quad (4)$$

$$= \begin{bmatrix} NM^{-1} \\ I \end{bmatrix} (I + CNM^{-1})^{-1} (CNM^{-1} + I)M \quad (5)$$

$$= \begin{bmatrix} NM^{-1} \\ I \end{bmatrix} M \quad (6)$$

$$= \begin{bmatrix} N \\ M \end{bmatrix} \quad (7)$$

Eq. (7) represents the merit of the proposed two degree-of-freedom control design where the feedback controller C does not appear neither in the trajectory tracking transfer function nor in the control effort transfer function. Therefore no limitation, in the tracking performance or the required actuators actions, results from the controller. In this case, nominally, the trajectory tracking performance can be designed independently from the feedback controller and therefore one can increase the bandwidth with no overshooting. This desired feature cannot be guaranteed by any single degree-of-freedom control design. For instance, for the case of feedback-only control, i.e., $X = 0$ and $Y = I$, the design criteria matrix becomes:

$$T_{\text{Fb}} = \begin{bmatrix} P(I + CP)^{-1}C \\ (I + CP)^{-1}C \end{bmatrix} \quad (8)$$

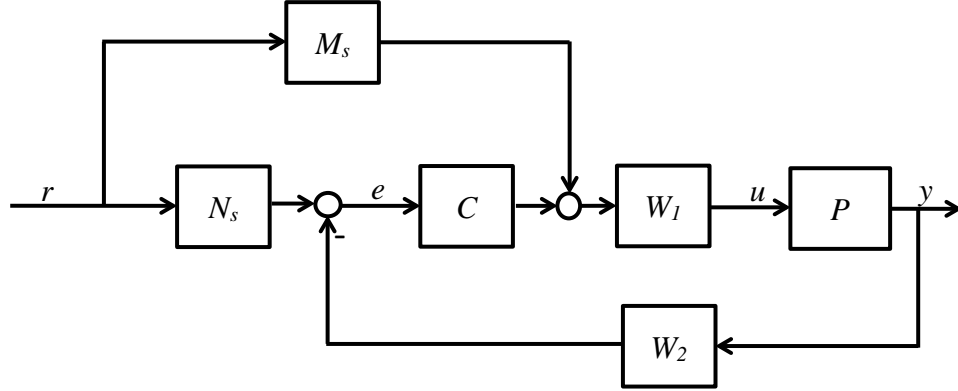


Figure 2. Equivalent control structure with shaping weights.

Eq. (8) includes limitations of the feedback loop. These limitations are well known and documented in literature, see for example [23]. The summary of these limitations is that there is a compromise between the bandwidth and the tracking performance, i.e., in order to achieve good trajectory tracking with no divergence, the bandwidth needs to be low which means slow manoeuvrability of the UAV. On the other hand, high bandwidth necessitates overshoot and divergence from the trajectory.

A. The Reference and Feedforward Filters

Coprime factorisation over \mathcal{RH}_∞ is the focal point in the proposed control design to synthesise the reference and feedforward filters. The filters X and Y are designed using the coprime factors of the linearised UAV model. Coprime factorisation over \mathcal{RH}_∞ is not unique and it has been shown in [29] that normalised coprime factorisation represents a good choice for the Ff/Fb control over other coprime factorisations such as inner-outer factorisation. This choice is specifically obvious for disturbed and uncertain systems which is the case of UAVs. Therefore, in this paper the right normalised coprime factorisation is utilised.

A right coprime factorisation $P = NM^{-1}$ is "normalised" if $N^*N + M^*M = I$ where N^* and M^* are the complex conjugate transpose of N and M respectively. This definition ensures that the block matrix $\begin{bmatrix} N \\ M \end{bmatrix}$ is inner which in turns induces specific frequency domain properties. For instance, if the linearised system P has high-gain at low frequencies and small-gain at high frequencies with good slope at cross-over frequency, the resulting N will have unity gain at low frequencies with similar bandwidth to P and low gain at high frequencies. The factor M will have gain close to unity at high frequencies and small gain at low frequencies. From Eq. (7), it can be seen that in the nominal case, the tracking performance of the UAV depends solely on the characteristics of N while the control effort depends only on the characteristics of M . This implies that for good tracking performance and enhanced control effort, the frequency response of the linearised system should be shaped so that we can guarantee the desirable frequency domain properties of N and M . The linearised system can be shaped using pre and/or post weighting functions W_1 and W_2 . The weights are designed using the standard loop shaping criteria described in [23] whereas the shaped system should have high gain at low frequencies, low gain at high frequencies and a smooth transition at

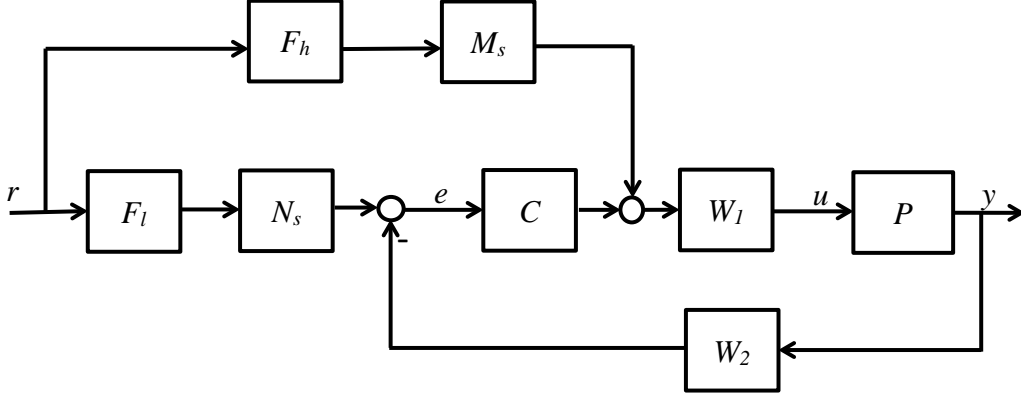


Figure 3. Equivalent control structure with shaping weights and phase compensation filters.

the crossover frequency with a slope of -20 dB/decade. These weights need to be considered in the final implementation of the controller. Figure 2 depicts the equivalent control structure when using the shaping weights W_1 and W_2 . Then, the feedforward and reference filters should be designed such as $X = M_s$ and $Y = N_s$, where $P_s = N_s M_s^{-1} = W_2 P W_1$.

B. The Phase Compensators

Given that the tracking performance and actuators effort are characterised only by N_s and M_s , a low and a high pass filter might be needed in the structure to account for any phase deterioration of N_s and M_s , see Figure 3. This is due to the fact that for single degree-of-freedom control, we pay attention only to the magnitude when shaping the system while the phase is taken care of by the feedback controller. In the case of the proposed Ff/Fb control, the feedback controller will have no effect on the transfer function matrix T and hence the phase of N_s and M_s should be considered explicitly as shown in Figure 3.

Using the low pass filter F_l to compensate for the phase of N_s and the high pass filter F_h to compensate for the phase of M_s will give:

$$T_{\text{Ff/Fb}} = \begin{bmatrix} P_s(I + CP_s)^{-1}(CN_s F_l + M_s F_h) \\ (I + CP_s)^{-1}(CN_s F_l + M_s F_h) \end{bmatrix} \quad (9)$$

In low frequency region, we have:

$$\overline{\sigma}(F_h) \ll 1, \overline{\sigma}(M_s) \ll 1 \text{ and } \underline{\sigma}(CP_s) \gg 1$$

where $\overline{\sigma}(\cdot)$ and $\underline{\sigma}(\cdot)$ are consequently the largest and smallest singular value of the corresponding transfer function. This enables us to write in low frequencies:

$$(I + CP_s) \approx CP_s \text{ and } (CN_s F_l + M_s F_h) \approx CN_s F_l$$

Therefore, in low frequency region, Eq.(9) can be written as:

$$T_{\text{Ff/Fb}} = \begin{bmatrix} P_s(CP_s)^{-1}CN_sF_l \\ (CP_s)^{-1}CN_sF_l \end{bmatrix} \quad (10)$$

$$= \begin{bmatrix} N_sF_l \\ M_sF_l \end{bmatrix} \quad (11)$$

In high frequency region, we have:

$$\overline{\sigma}(F_l) \ll 1, \underline{\sigma}(N_s) \ll 1 \text{ and } \overline{\sigma}(CP_s) \ll 1$$

This enables us to write:

$$(I + CP_s) \approx I \text{ and } (CN_sF_l + M_sF_h) \approx M_sF_h$$

Therefore, Eq. (9) can be written in high frequency region as:

$$T_{\text{Ff/Fb}} = \begin{bmatrix} N_sM_s^{-1}M_sF_h \\ M_sF_h \end{bmatrix} \quad (12)$$

$$= \begin{bmatrix} N_sF_h \\ M_sF_h \end{bmatrix} \quad (13)$$

For simplicity of representation and because N_s and M_s are of interest to the designer only in low frequencies and high frequencies respectively, Eqs. (11)- (13) can be combined in one approximation as:

$$T_{\text{Ff/Fb}} \approx \begin{bmatrix} N_sF_l \\ M_sF_h \end{bmatrix} \quad (14)$$

It is worth mentioning that the structure of the required low pass and high pass filters F_l and F_h - if needed - depends mainly on the frequency response of the original system P .

C. The Feedback Controller

The feedback controller C can be designed using any known method in literature. The feedback controller is synthesised to stabilise the system and hence it should be designed irrespective of the feedforward and reference filters X and Y . Generally speaking, UAVs are MIMO coupled systems and therefore, it is preferable to use a robust MIMO control method such as \mathcal{H}_∞ Loop Shaping Design Method (LSDM). In addition, the fact that the loop will be already shaped for the design of the filters X and Y makes the \mathcal{H}_∞ LSDM an ideal control design candidate. However, the proposed Ff/Fb approach is still valid for any other established control technique. In the examples presented in this paper, \mathcal{H}_∞ LSDM is used for the synthesis of the feedback controller.

D. An Illustration Example

To demonstrate the concept of the proposed Ff/Fb control, we will consider a simple mathematical example. This example represents a guideline to practitioners on how to design and implement the Ff/Fb control.

Consider a SISO system of double integrator $P = \frac{1}{s^2}$. In order to synthesize the Ff/Fb controller, we shape the system by a pre compensator of $W_1 = \frac{10.5(s+0.6)}{s+8}$. The selection of W_1 is based on the standard shaping criteria discussed in Section II-A. Figure 4 demonstrates the frequency response of the original system P and the shaped system $P_s = W_1P$.

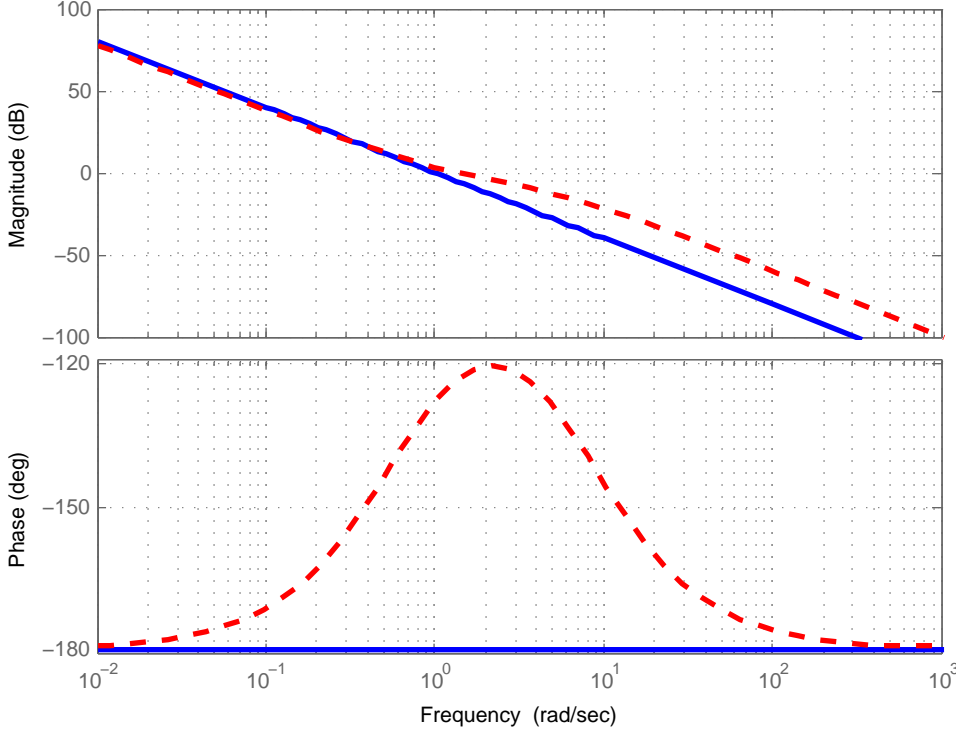


Figure 4. Frequency response of the original system P (solid blue) and the shaped system $P_s = W_1P$ (dashed red) for a SISO double integrator system.

Figure 5 demonstrates the frequency response of the shaped system P_s and its normalised coprime factors N_s and M_s where $P_s = W_1P = N_sM_s^{-1}$. We can see clearly that the magnitudes of N_s and M_s are good for ideal tracking performance and control effort respectively. However, the phase needs some compensation via low pass filter and high pass filter respectively as discussed before. The choice of F_l and F_h depends only on the required phase correction of N_s and M_s . Figure 5 shows that in low frequencies the phase of N_s needs correction by $-\pi$. Similarly in high frequencies, the phase of M_s needs correction by π . Therefore in order to design the Ff/Fb control for this single SISO system, we add a low pass filter of $F_l = \frac{-1}{0.01s+1}$ so that we can compensate the phase of the tracking performance of the closed loop system. Similarly, a high pass filter of $F_h = \frac{-s^2}{s^2+0.2s+0.01}$ should be added to the feedforward path in order to compensate for the phase of the coprime factor M_s . We complete the Ff/Fb control design by synthesising an \mathcal{H}_∞ controller for the feedback loop. To show the advantages of the proposed Ff/Fb control method over a single degree-of-freedom control, we also include in the results the design of the closed loop feedback-only control using the same \mathcal{H}_∞ controller. We use \mathcal{H}_∞ norm to analyse the difference between the two controllers with regard to the design criteria. The \mathcal{H}_∞ norm of a transfer function G is defined in [23] as the essential supremum singular value of the transfer function over all frequencies:

$$\|G\|_{\infty} = \operatorname{ess\,sup}_{\omega} \overline{\sigma}(G(j\omega))$$

In this paper, we will use the value $20\log_{10}(\|G\|_{\infty})$ to make the reading of \mathcal{H}_{∞} norm compatible with the plotting of the frequency response. For the tracking transfer function, the value $20\log_{10}(\|T_{11}\|_{\infty})$ above 0 indicates the overshoot of the closed loop system over all frequencies. For the control effort transfer function, the value $20\log_{10}(\|T_{12}\|_{\infty})$ represents the maximum excitation of the actuators over all frequencies where T is the closed loop transfer function matrix as defined in Eqs. (8) and (14) and $T_{11} = T_{ry}$, $T_{12} = T_{ru}$.

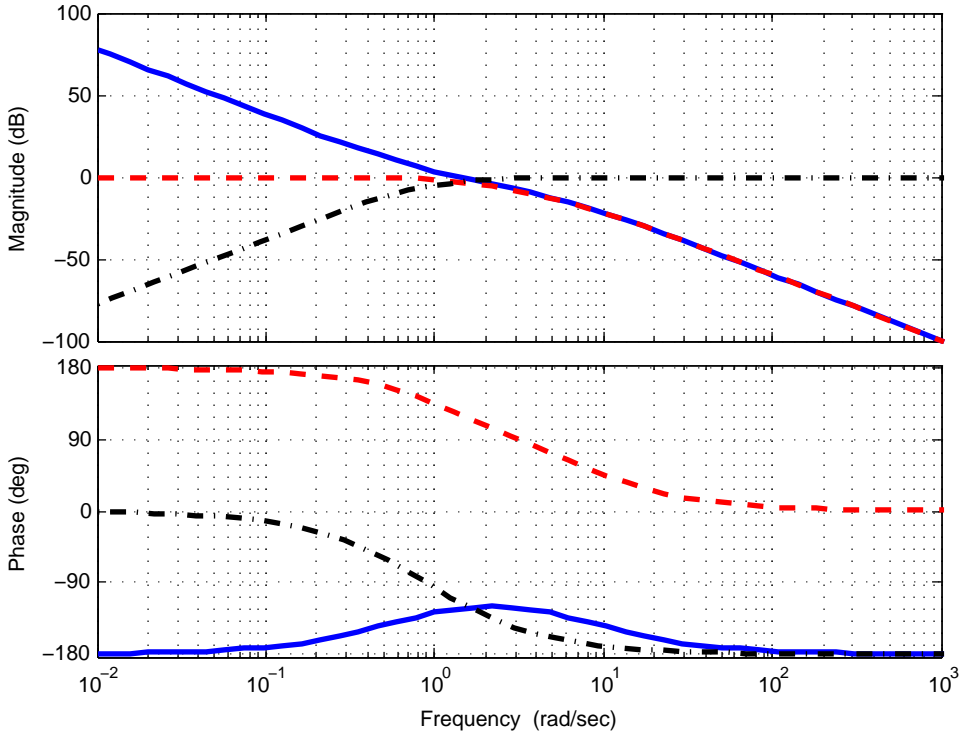


Figure 5. Frequency response of the shaped system (solid blue), and the normalised coprime factors N_s (dashed red) and M_s (dashed-dotted black), the illustration example.

Figure 6 shows the frequency response of the closed loop tracking transfer function for the designed Ff/Fb control. The figure also contains the frequency response of the closed loop feedback-only control using the same \mathcal{H}_{∞} controller. It can be noticed clearly that both systems have identical bandwidth, however, around the roll-off frequency there is a small peak in the case of feedback-only control. This peak reflects an overshoot in the time domain response as demonstrated in Figure 7.

Figure 8 shows the frequency response of the reference-to-input transfer function for both cases, the single degree-of-freedom feedback-only control and the Ff/Fb control. Figure 9 shows the step response of the reference-to-input transfer function for both cases. These two figures show that the excitation of the actuators for the case of the Ff/Fb is less which means less control effort and this is a desirable feature. The superiority of the Ff/Fb control over feedback-only control can be confirmed by the \mathcal{H}_{∞} norm of the

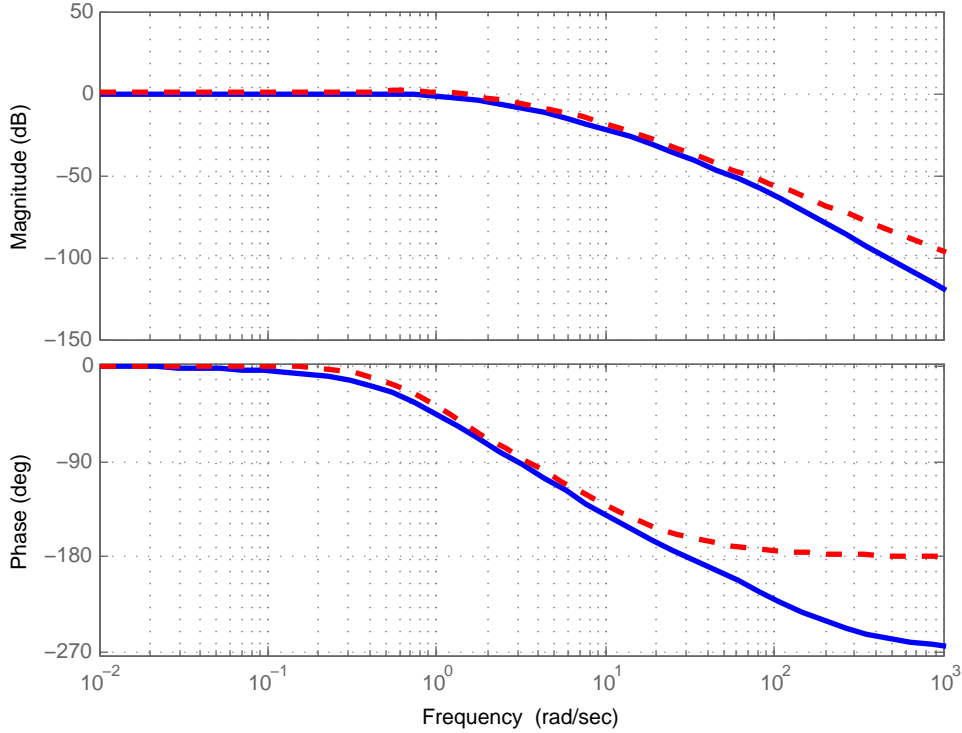


Figure 6. Frequency response of the tracking transfer function (reference-to-output) of the closed loop system for two cases: the Ff/Fb control (solid blue) and single degree-of-freedom feedback-only control (dashed red), the illustration example.

closed loop transfer functions for both cases whereas we have:

$$\text{for Ff/Fb: } \begin{bmatrix} 20\log_{10}(\|T_{ry}\|_{\infty}) \\ 20\log_{10}(\|T_{ru}\|_{\infty}) \end{bmatrix} = \begin{bmatrix} 0 \\ 0 \end{bmatrix}$$

and

$$\text{for Fb: } \begin{bmatrix} 20\log_{10}(\|T_{ry}\|_{\infty}) \\ 20\log_{10}(\|T_{ru}\|_{\infty}) \end{bmatrix} = \begin{bmatrix} 1.3487 \\ 3.4231 \end{bmatrix}$$

These values of the \mathcal{H}_{∞} norm indicates that the Ff/Fb control has no overshoot while the feedback only control has an overshoot of 1.3 dB. The actuators excitation for the feedback-only control is higher by 3.4 dB.

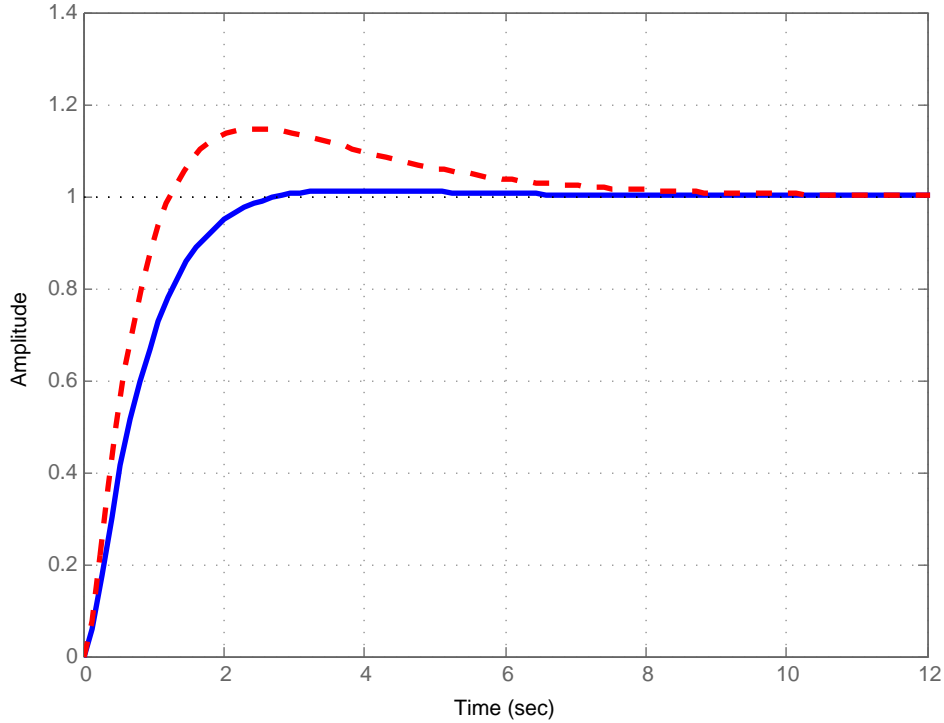


Figure 7. Step response of the tracking transfer function (reference-to-output) of the closed loop system for two cases: the Ff/Fb control (solid blue) and single degree-of-freedom feedback-only control (dashed red), the illustration example.

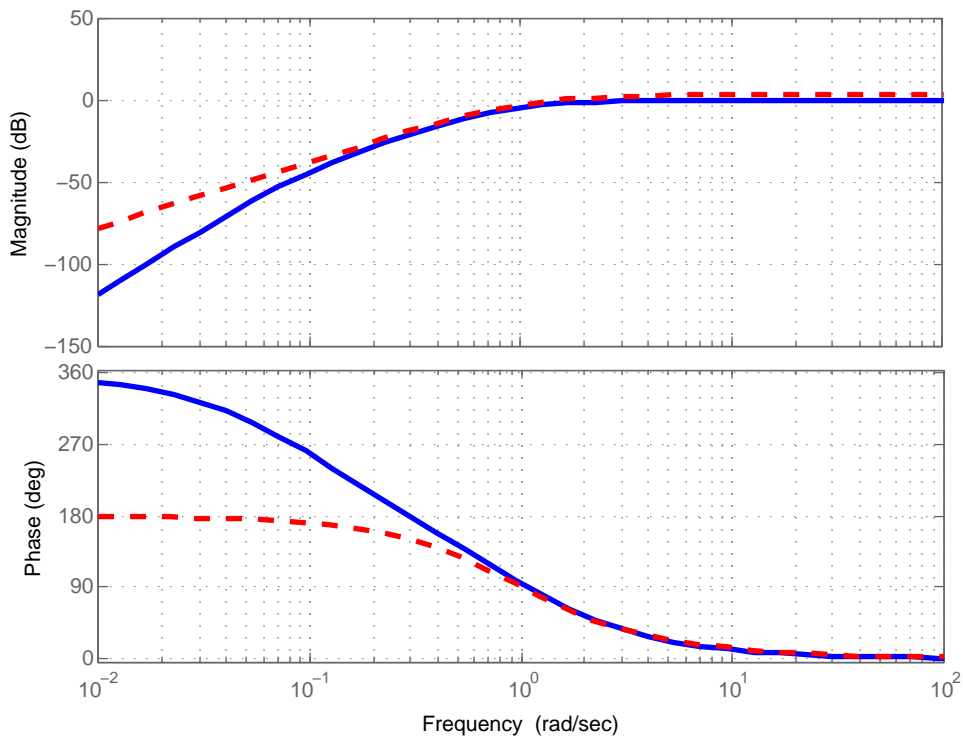


Figure 8. Frequency response of the control effort (reference-to-input) transfer function for two cases: the Ff/Fb control (solid blue) and single degree-of-freedom feedback-only control (dashed red), the illustration example.

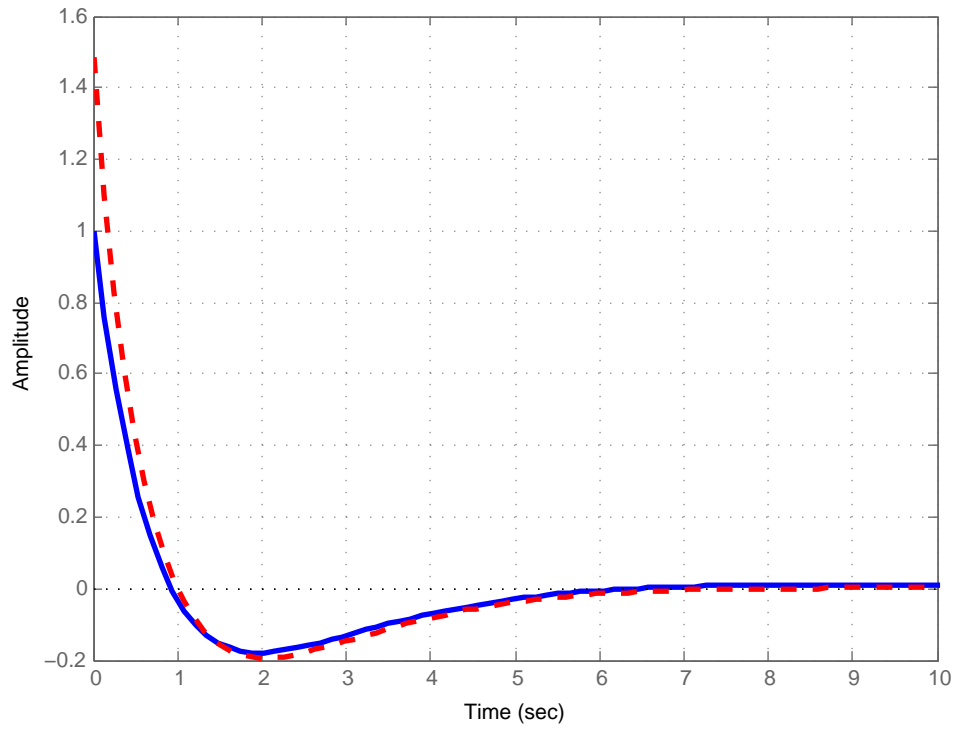


Figure 9. Step response of the control effort transfer function of the closed loop system for two cases: the Ff/Fb control (solid blue) and single degree-of-freedom feedback-only control (dashed red), the illustration example.

III. CASE I: A FULLY ACTUATED TRI-ROTOR UAV

In this section, the proposed control method is designed for a tri-rotor UAV in Simulation. Figure 10 shows a diagram of the UAV. The vehicle is proposed in [30] with six degree-of-freedom and a symmetric shape where its body is composed of three identical rotors rotating in the same direction and three identical servo motors that control the tilting angles of the rotors independently. The position and orientation of the vehicle can be controlled separately through the six inputs, i.e., speeds of three electric DC motors and angles of three servo motors. Full description of the vehicle and details about the derivation of its nonlinear model can be found in [30], [31], [32].

A. The Model

Following the derivation of [32], the full model of the UAV including actuator dynamics is expressed in Eqs. (15) - (20):

$$\dot{\mathbf{v}}_v^b = g\mathbf{H}_g - \mathcal{S}(\boldsymbol{\omega}_v^b)\mathbf{v}_v^b + \frac{k_f}{M_{tot}}\mathbf{H}_f\rho \quad (15)$$

$$\dot{\boldsymbol{\omega}}_v^b = -(\mathbf{I}_v^b)^{-1}\mathcal{S}(\boldsymbol{\omega}_v^b)\mathbf{I}_v^b\boldsymbol{\omega}_v^b + (\mathbf{I}_v^b)^{-1}(k_f\mathbf{H}_t - k_t\mathbf{H}_f)\rho \quad (16)$$

$$\dot{\boldsymbol{\eta}}_v = \boldsymbol{\Psi}\boldsymbol{\omega}_v^b \quad (17)$$

$$\dot{\boldsymbol{\lambda}}_v^e = \mathbf{R}_b^e\mathbf{v}_v^b \quad (18)$$

$$\dot{\mathbf{x}}_a = \mathbf{A}_a\mathbf{x}_a + \mathbf{B}_a\mathbf{u}_a \quad (19)$$

$$\mathbf{y}_a = \mathbf{x}_a \quad (20)$$

Table I defines all terms used in the model of the UAV. The model is written in a compact form where each state variable has a dimension and defined as following:

$$\mathbf{v}_v^b = \begin{bmatrix} u \\ v \\ w \end{bmatrix}, \boldsymbol{\omega}_v^b = \begin{bmatrix} p \\ q \\ r \end{bmatrix}, \boldsymbol{\eta}_v = \begin{bmatrix} \phi_v \\ \theta_v \\ \psi_v \end{bmatrix}, \boldsymbol{\lambda}_v^e = \begin{bmatrix} x_v \\ y_v \\ z_v \end{bmatrix}, \quad (21)$$

and for the actuator dynamics we have:

$$\mathbf{x}_a = \begin{bmatrix} \boldsymbol{\omega}_{m_1} \\ \boldsymbol{\omega}_{m_2} \\ \boldsymbol{\omega}_{m_3} \\ \alpha_{s_1} \\ \alpha_{s_2} \\ \alpha_{s_3} \end{bmatrix}, \mathbf{u}_a = \begin{bmatrix} V_{m_1} \\ V_{m_2} \\ V_{m_3} \\ V_{s_1} \\ V_{s_2} \\ V_{s_3} \end{bmatrix}, \mathbf{A}_a = \begin{bmatrix} c_m\mathbf{I} & \mathbf{0} \\ \mathbf{0} & c_s\mathbf{I} \end{bmatrix}, \mathbf{B}_a = \begin{bmatrix} k_m\mathbf{I} & \mathbf{0} \\ \mathbf{0} & k_s\mathbf{I} \end{bmatrix}. \quad (22)$$

The remaining matrices are defined as:

$$\mathbf{H}_f = \begin{bmatrix} 0 & -\frac{\sqrt{3}}{2} & \frac{\sqrt{3}}{2} & 0 & 0 & 0 \\ 1 & -\frac{1}{2} & \frac{1}{2} & 0 & 0 & 0 \\ 0 & 0 & 0 & 1 & 1 & 1 \end{bmatrix}, \mathbf{H}_g = \begin{bmatrix} \sin(\theta_v) \\ -\sin(\theta_v)\cos(\theta_v) \\ -\cos(\phi_v)\cos(\theta_v) \end{bmatrix} \quad (23)$$

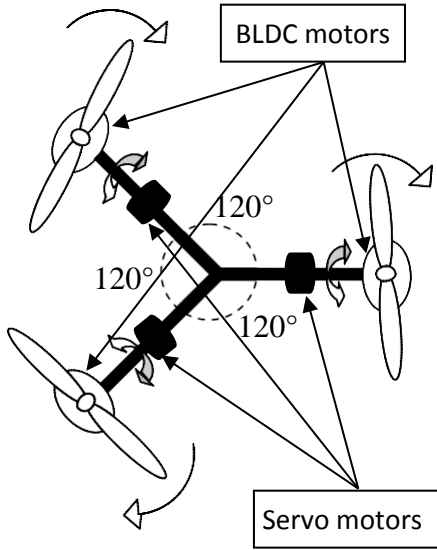


Figure 10. Diagram of the Tri-rotor UAV (top view), taken from [31] with some adaptations.

$$H_t = \begin{bmatrix} 0 & 0 & 0 & 0 & \frac{\sqrt{3}}{2} & -\frac{\sqrt{3}}{2} \\ 0 & 0 & 0 & -1 & \frac{1}{2} & \frac{1}{2} \\ 1 & 1 & 1 & 0 & 0 & 0 \end{bmatrix}, \rho = \begin{bmatrix} \omega_{m_1}^2 \sin(\alpha_{s_1}) \\ \omega_{m_2}^2 \sin(\alpha_{s_2}) \\ \omega_{m_3}^2 \sin(\alpha_{s_3}) \\ \omega_{m_1}^2 \cos(\alpha_{s_1}) \\ \omega_{m_2}^2 \cos(\alpha_{s_2}) \\ \omega_{m_3}^2 \cos(\alpha_{s_3}) \end{bmatrix}. \quad (24)$$

The matrix $S(\omega_v^b)$ is the skew matrix of the vector ω_v^b . The matrix Ψ is defined as the rotational matrix between the angular velocity ω_v^b expressed in the body coordinate system and the angular velocity η_v related to the earth coordinate system. The matrix R_b^e is the rotational matrix from the body coordinate system to the earth coordinate system. The definition of these rotational matrices along with their mathematical expressions are well defined in literature, see for example [33] for details.

B. Feedback Linearisation

To linearise the nonlinear model, an input-output feedback linearisation technique is used. The resulting linearised system is a chain of three integrators and the associated feedback linearisation law is:

$$u_a = \beta^{-1} (\vartheta - C_1 \rho - C_2), \quad (25)$$

where

$$\beta = \begin{bmatrix} \Psi I^{-1} (k_f H_t - k_t H_f) \\ \frac{k_f}{M_{tot}} R_b^e H_f \end{bmatrix} N B_a, \quad (26)$$

$$C_1 = \begin{bmatrix} (2\Psi I^{-1} - \Psi I^{-1} S(\omega) + \Psi I^{-1} S(I\omega) I^{-1}) (k_f H_t - k_t H_f) \\ \frac{k_f}{M_{tot}} R_b^e S(\omega) H_f \end{bmatrix}, \quad (27)$$

symbol	definition
ω_{m_i}	rotational speed of the i^{th} DC motor
V_{m_i}	input voltage of the i^{th} DC motor
α_{s_i}	tilting angle of the i^{th} servo motor
V_{s_i}	input voltage of the i^{th} servo motor
k_f	thrust-to-speed constant of the propeller
k_t	torque-to-speed constant of the propeller
g	gravitational acceleration
M_{tot}	total mass of the UAV
I_v	inertia matrix of the UAV
v_v	the transitional velocity of the UAV
u, v, w	the Cartesian coordinates of the UAV transitional velocity
ω_v	angular velocity of the UAV
p, q, r	the Cartesian coordinates of the UAV angular velocity
η	attitude vector of the UAV related to the earth frame
λ^e	position vector of the UAV (earth frame)
ϕ_v	roll angle of the UAV related to the earth frame
θ_v	pitch angle of the UAV related to the earth frame
ψ_v	yaw angle of the UAV related to the earth frame
x_v	the x coordinate position of the UAV in the earth frame
y_v	the y coordinate position of the UAV in the earth frame
z_v	altitude of the UAV in the earth frame
R_b^e	the rotational matrix from frame b to frame e
b	superscript/subscript denotes the body Cartesian coordinate system
e	superscript/subscript denotes the earth Cartesian coordinate system
c_m	the time constant of the DC motor response
c_s	time constant of the servo motor response
k_m	gain of the DC motor (input voltage to the speed)
k_s	gain of the servo motor (input voltage to tilting angle)
I	unity matrix of suitable dimension
$\mathbf{0}$	zero matrix of suitable dimension

Table 1

NOTATIONS OF THE TRI-ROTOR UAV MODEL

$$C_2 = \begin{bmatrix} (\ddot{\Psi} - 2\dot{\Psi}I^{-1}S(\omega)I - \Psi I^{-1}S(I\omega)I^{-1}S(\omega)I) \omega \\ gR_b^e S(\omega)H_g \end{bmatrix} + \begin{bmatrix} (\Psi I^{-1}S(\omega)S(\omega)I) \omega \\ gR_b^e H_{dg} \Psi \omega \end{bmatrix} + \begin{bmatrix} \Psi I^{-1} (k_f H_t - k_t H_f) \\ \frac{k_f}{M_{tot}} R_b^e H_f \end{bmatrix} NA_a x_a, \quad (28)$$

$$N = \begin{bmatrix} \text{diag}(2\omega_{m_i} \sin \alpha_{s_i}) & \text{diag}(\omega_{m_i}^2 \cos \alpha_{s_i}) \\ \text{diag}(2\omega_{m_i} \cos \alpha_{s_i}) & \text{diag}(-\omega_{m_i}^2 \sin \alpha_{s_i}) \end{bmatrix}_{6 \times 6}, \quad i = 1, 2, 3 \quad (29)$$

$$H_{dg} = \begin{bmatrix} \cos(\theta_v) & 0 & 0 \\ \sin(\theta_v) \sin(\phi_v) & -\cos(\phi_v) \cos(\theta_v) & 0 \\ \cos(\theta_v) \sin(\phi_v) & \sin(\phi_v) \cos(\theta_v) & 0 \end{bmatrix}, \quad (30)$$

and \mathcal{D} is the new artificial input vector. The term *diag* in matrix N refers to the diagonal structure of the matrix.

C. Simulation Results

To implement the Ff/Fb control and achieve the control design criteria in terms of fast tracking with no overshoot and control effort with no saturation, the linearised system needs to be shaped first using pre and post weights W_1 and W_2 . These weights have then to be included in the final implementation of the control system as shown in Figure 2. To design W_1 and W_2 , we follow the standard loop shaping criteria mentioned in Section II-A whereas the shaped system should have high gain at low frequencies, low gain at high frequencies and a smooth transition at the crossover frequency with a slop of -20 dB/decade. The linearised UAV system is diagonal and has sufficiently low gain at high frequencies, so we can put $W_2 = I$ and use $W_1 = \frac{105s^2+126s+37.8}{s^2+16s+64} I_{6 \times 6}$ to shape the system. Figure 11 depicts the singular values plot of the linearised system and the shaped system. As discussed in the illustration example, a low and high pass filters are needed to compensate for the phase of N_s and M_s . We use the filters $F_l = \frac{-1}{0.01s+1}$ to compensate the phase of N_s by $-\pi$ and a high pass filter of $F_h = \frac{-s^2}{s^2+0.2s+0.01}$ to compensate the phase of M_s by π . Now, the reference and feedforward filters can be designed using the normalised coprime factorisation of the shaped systems such that $X = M_s F_h$ and $Y = N_s F_l$ where $P_s = N_s M_s^{-1} = P W_1$.

The feedback controller C is synthesised to ensure the internal stability of the closed loop and guarantee the robustness of the system against disturbances and uncertainties. For the UAV in hand, we employ the \mathcal{H}_∞ LSDM to design the feedback controller. Justification for the use of the \mathcal{H}_∞ LSDM in UAV systems lies in the fact that UAVs are MIMO systems that are susceptible to high level of uncertainties and disturbances due to the nonlinear dynamics. This makes the \mathcal{H}_∞ LSDM an ideal candidate for the feedback control synthesis. The implementation of \mathcal{H}_∞ LSDM in UAVs is well established in literature and shows good results, see for example [34], [35], [36]. For the example in hand, the achieved robust stability margin is 0.4365.

The designed Ff/Fb control applied to the tri-rotor UAV in Simulation. Figures 12 and 13 produce the singular values plot of the resulting tracking transfer function and control effort transfer function respectively. These figures also contain the resulting transfer functions in case of feedback-only control, where the same \mathcal{H}_∞ LSDP is implemented in a single degree-of-freedom control structure, i.e., $X = 0$ and $Y = I$. Figure 12 reflects the fact that the two control structure have similar bandwidth, however, for the case of feedback-only control, the tracking performance of the system contains an overshoot of about 5 dB. The author has tried to eliminate the overshoot by re-tuning the feedback controller which results in a reduced bandwidth of at least 25%. This overshoot does not exist in the proposed Ff/Fb control and the bandwidth is maintained. For the reference-to-input transfer function in Figure 13, it can be noted that the case of feedback-only control excites the actuators more than the case of the proposed Ff/Fb control which is undesirable and it could lead to actuator saturation. The \mathcal{H}_∞ norm of the closed loop transfer functions for both control design quantifies the advantages of the Ff/Fb over feedback-only control as following:

$$\text{for Ff/Fb: } \begin{bmatrix} 20\log_{10}(\|T_{ry}\|_\infty) \\ 20\log_{10}(\|T_{ru}\|_\infty) \end{bmatrix} = \begin{bmatrix} 0 \\ 0 \end{bmatrix}$$

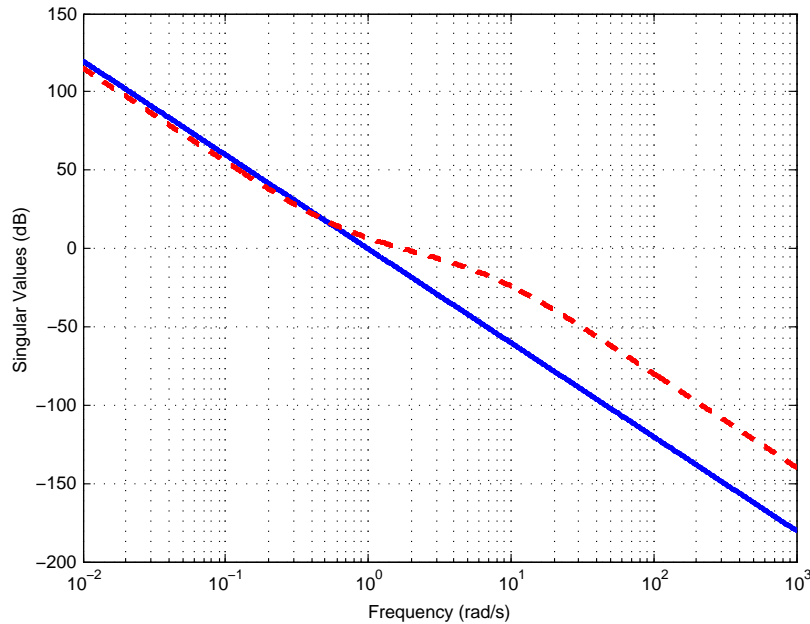


Figure 11. Singular values plot of the linearised model (solid) and the shaped model (dashed), the tri-rotor UAV.

and

$$\text{for Fb: } \begin{bmatrix} 20 \log_{10}(\|T_{ry}\|_{\infty}) \\ 20 \log_{10}(\|T_{ru}\|_{\infty}) \end{bmatrix} = \begin{bmatrix} 2.9441 \\ 2.5099 \end{bmatrix}$$

The values of the \mathcal{H}_{∞} norm shows that the feedback-only control excites the actuator more and has an overshoot while the Ff/Fb has no overshoot and has less control effort.

To further confirm the advantage of the proposed Ff/Fb control over feedback-only control, Figure 14 shows the frequency response of the closed loop reference-to-output transfer function, including both the magnitude and the phase, for the first channel. The other diagonal channels are identical where the system is very large 6×6 and it would be inappropriate to demonstrate the bode plot of the whole system. Similarly, Figure 15 shows the frequency response of the closed loop reference-to-input transfer function for the first channel. Both figures confirm that the Ff/Fb has no overshoot with similar bandwidth to the feedback-only control and causes less excitation to the actuators.

A scenario of rising curved trajectory tracking with the Ff/Fb control is shown in Figures 16 - 17 along with the actuators effort in Figure 18. The graphs show good trajectory tracking and the actuators are working within their physical restrictions of $\pm\pi/2$ for the servo angles and 10^4 RPM for the DC motor speed.

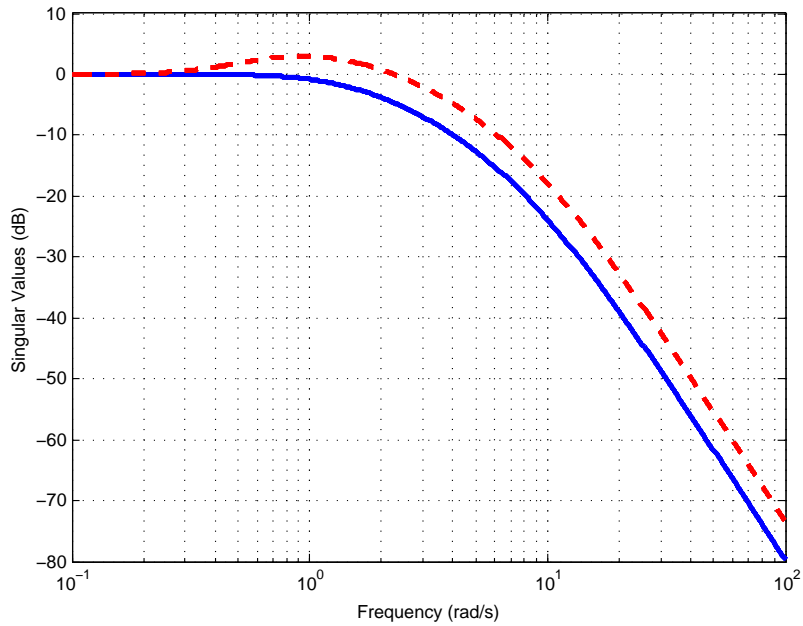


Figure 12. Singular values plot of the closed-loop reference-to-output tracking transfer function for the case of the Ff/Fb control (solid blue) and the feedback-only control (dashed red), the tri-rotor UAV.

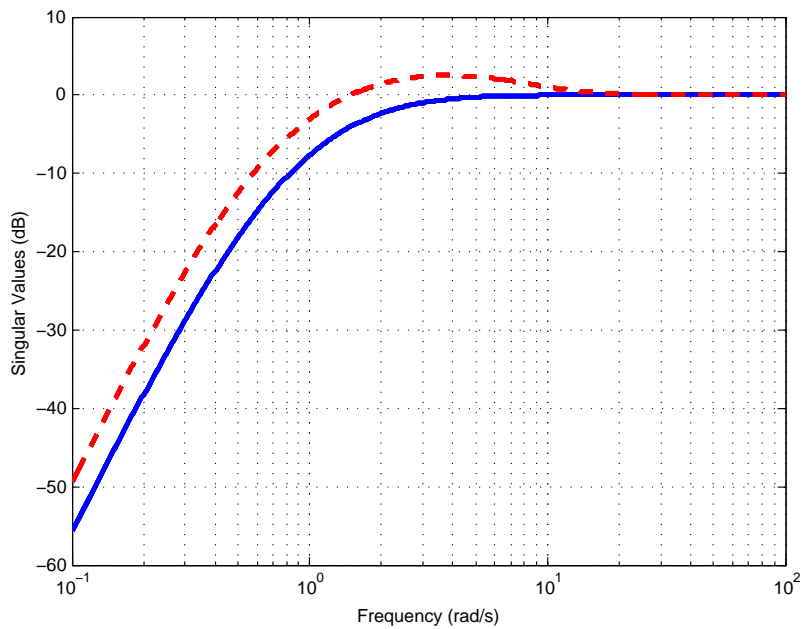


Figure 13. Singular values plot of the closed-loop reference-to-input transfer function for the case of the Ff/Fb control (solid blue) and the feedback-only control (dashed red), the tri-rotor UAV.

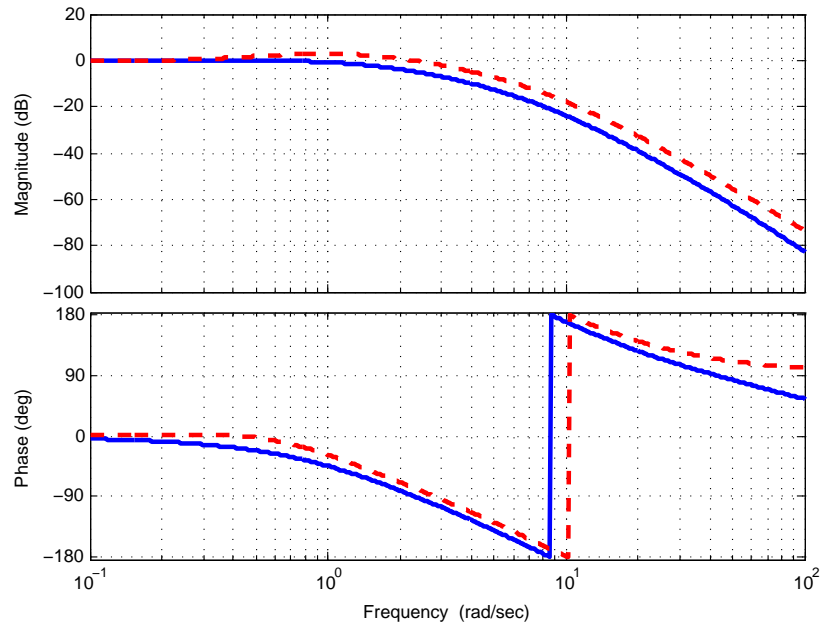


Figure 14. The frequency response of the closed-loop reference-to-output tracking for the first channel with the case of the Ff/Fb control (solid blue) and the feedback-only control (dashed red), the tri-rotor UAV.

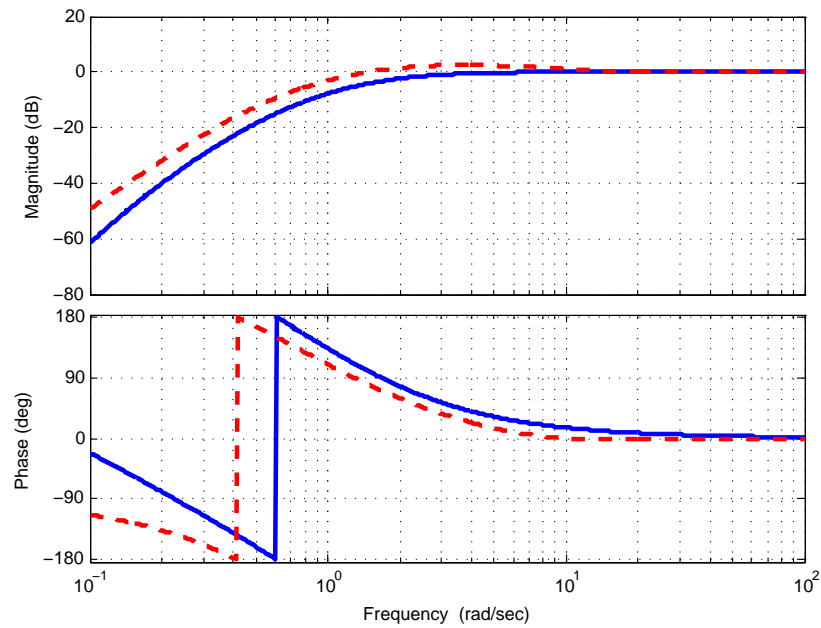


Figure 15. The frequency response of the closed-loop reference-to-input transfer function for the first channel with the case of the Ff/Fb control (solid blue) and the feedback-only control (dashed red), the tri-rotor UAV.

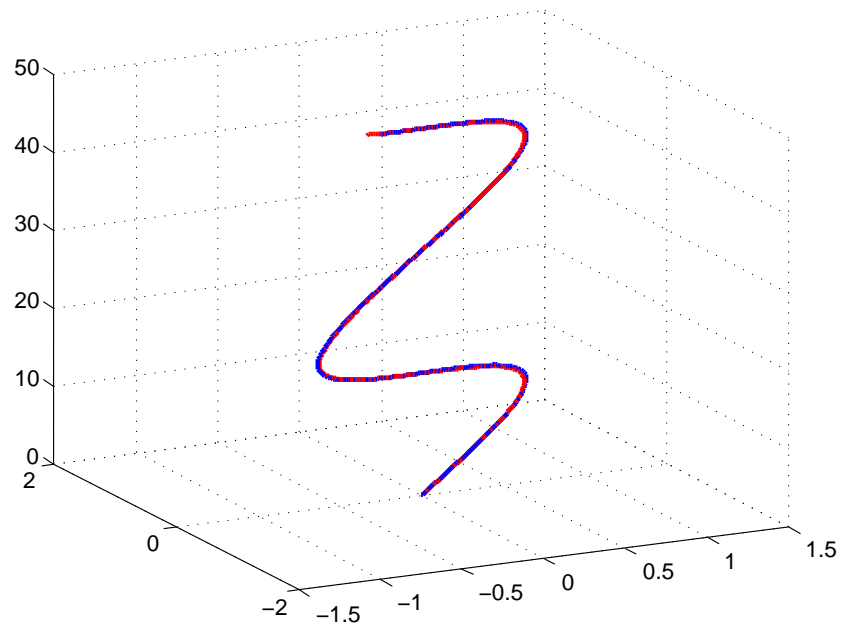


Figure 16. The 3D position (solid blue) of the tri-rotor UAV for a rising curved trajectory (dashed red).

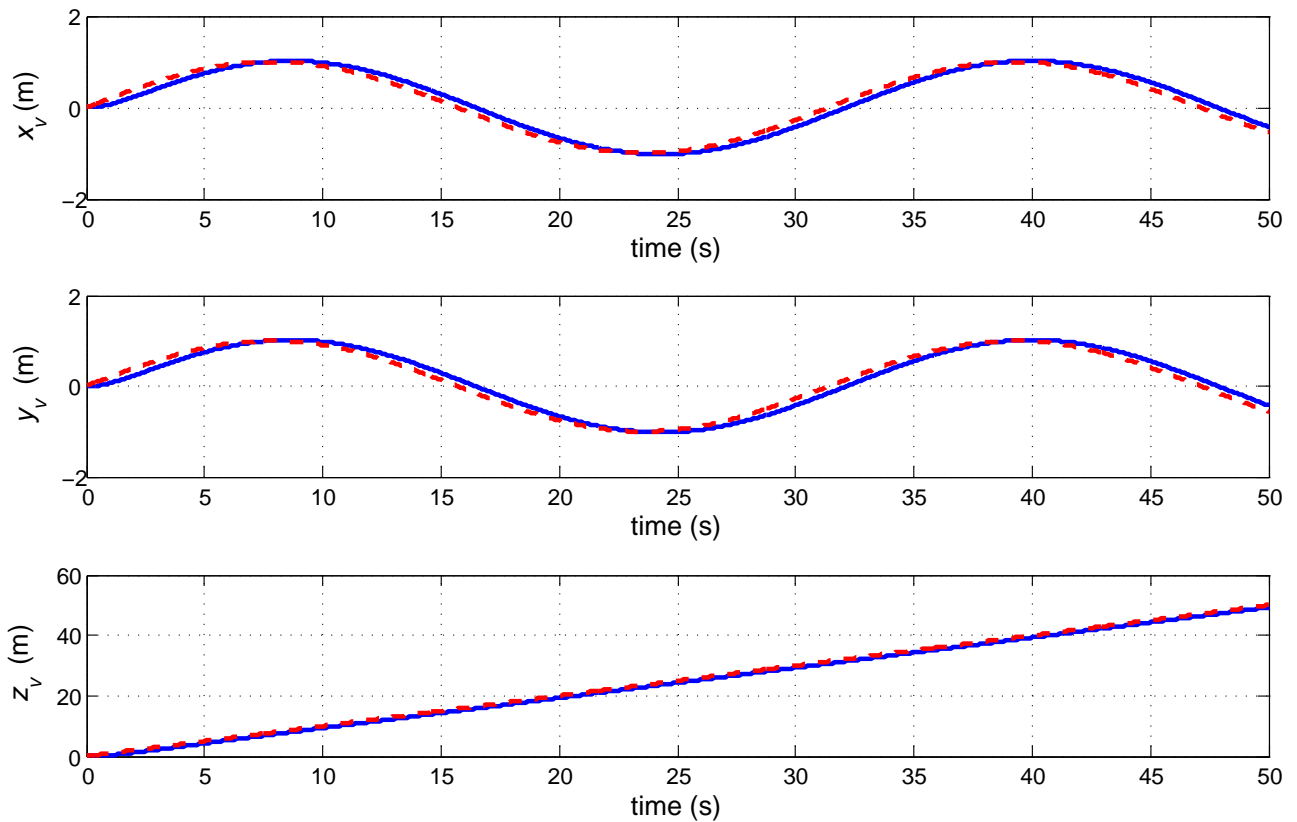


Figure 17. The Cartesian position (solid blue) of the tri-rotor UAV for a rising curved trajectory (dashed red).

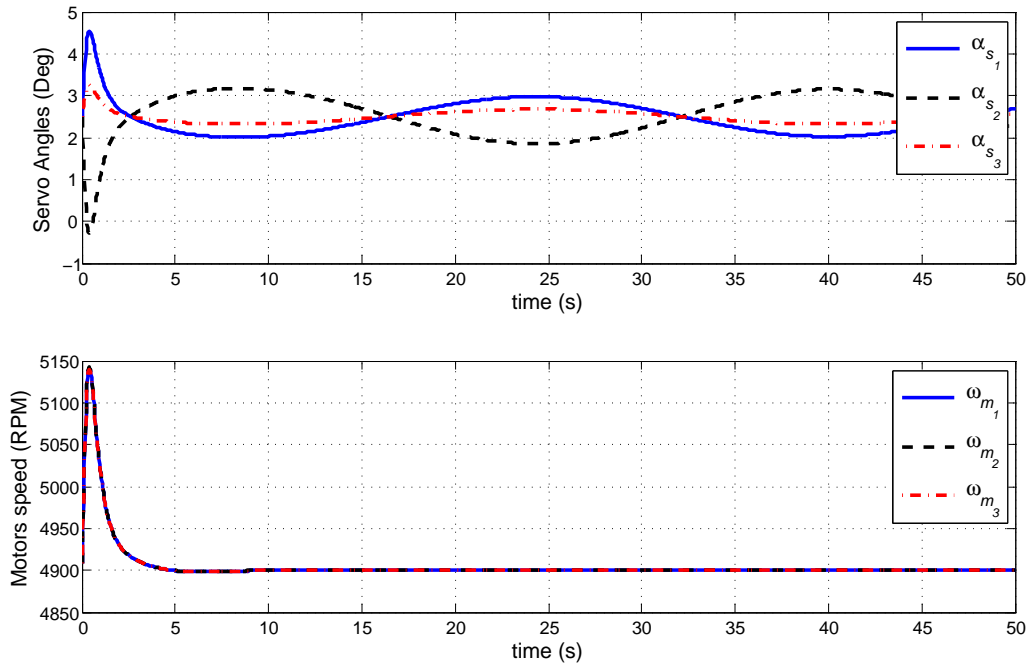


Figure 18. The angles of the servos (top) and the speed of the DC motors (bottom) for a rising curved flight, the tri-rotor UAV.

D. Uncertainty and Robustness

One of the main concern for controlling nonlinear UAV systems is the robustness of the system against disturbances and uncertainty. For instance, uncertainty in modelling the system makes the linearised system never linear. This fact adds further requirement to the control design to ensure robustness in hardware implementation. In order to present the robustness of the proposed control method, a stable second order multiplicative uncertainty has been introduced to the system and the same controller synthesised for the nominal case is tested again. Therefore, the tested uncertain system is:

$$P_u = P\Delta^2 \text{ with } \Delta = 1 + \frac{a}{s+b}$$

where $0 < a < 1$ and $0 < b < 1$ are random numbers and generated using Matlab random generator functions. Figures 19 - 20 show the performance of the Ff/Fb control under the model uncertainty with $\Delta^2 = \frac{s^2+3.504s+3.07}{s^2+1.1919s+0.9206}$. The controller accommodates the uncertainty and shows good tracking.

Another robustness aspect that should be considered for any control design is the input disturbances. In UAV systems, the input signal is susceptible to noise and disturbances. In order to present the robustness of the proposed Ff/Fb control method, an input disturbance within the range of $\pm 10\%$ of the input signal for the demonstrated trajectory is introduced in simulation. Figures 21 - 22 show the performance of the Ff/Fb control under the introduced input disturbances. The control system rejects the disturbances and maintain the trajectory tracking of the system.

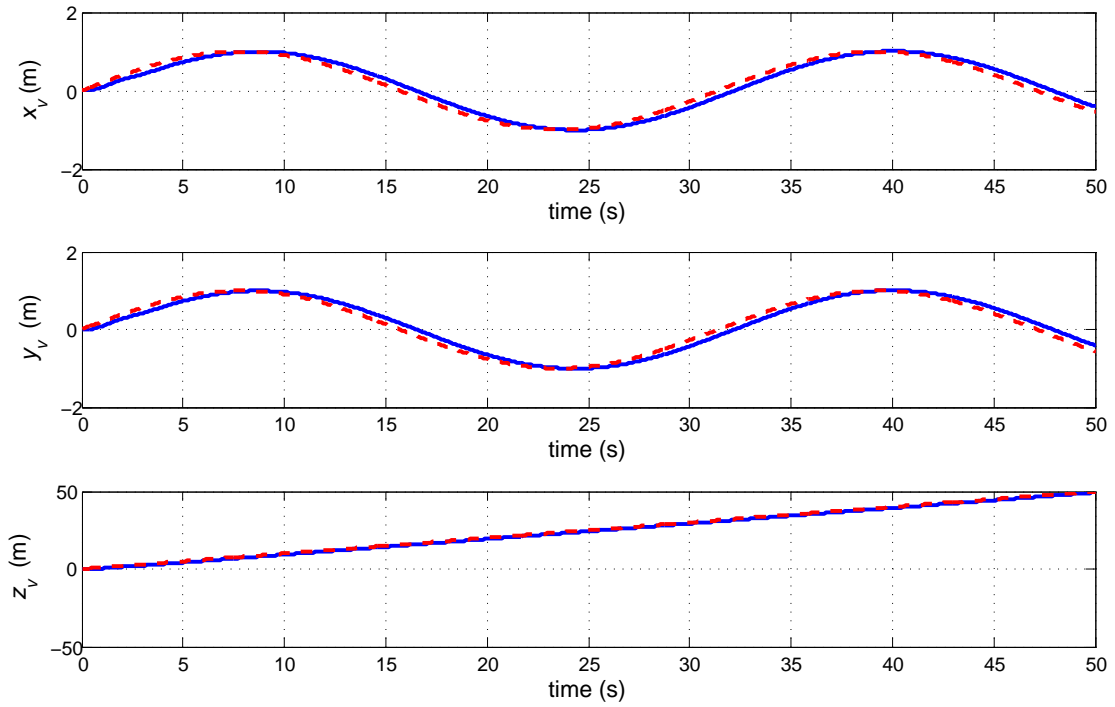


Figure 19. The Cartesian position (solid blue) of the tri-rotor UAV for a rising curved trajectory (dashed red) under model multiplicative uncertainty.

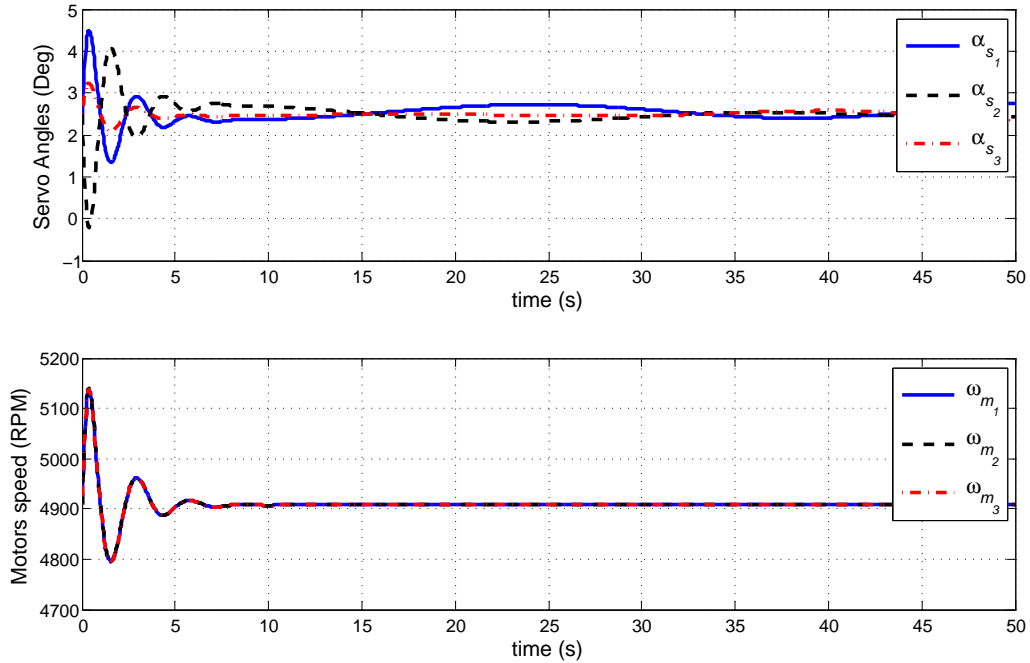


Figure 20. The angles of the servos (top) and the speed of the DC motors (bottom) for a rising curved flight under model multiplicative uncertainty, the tri-rotor UAV.

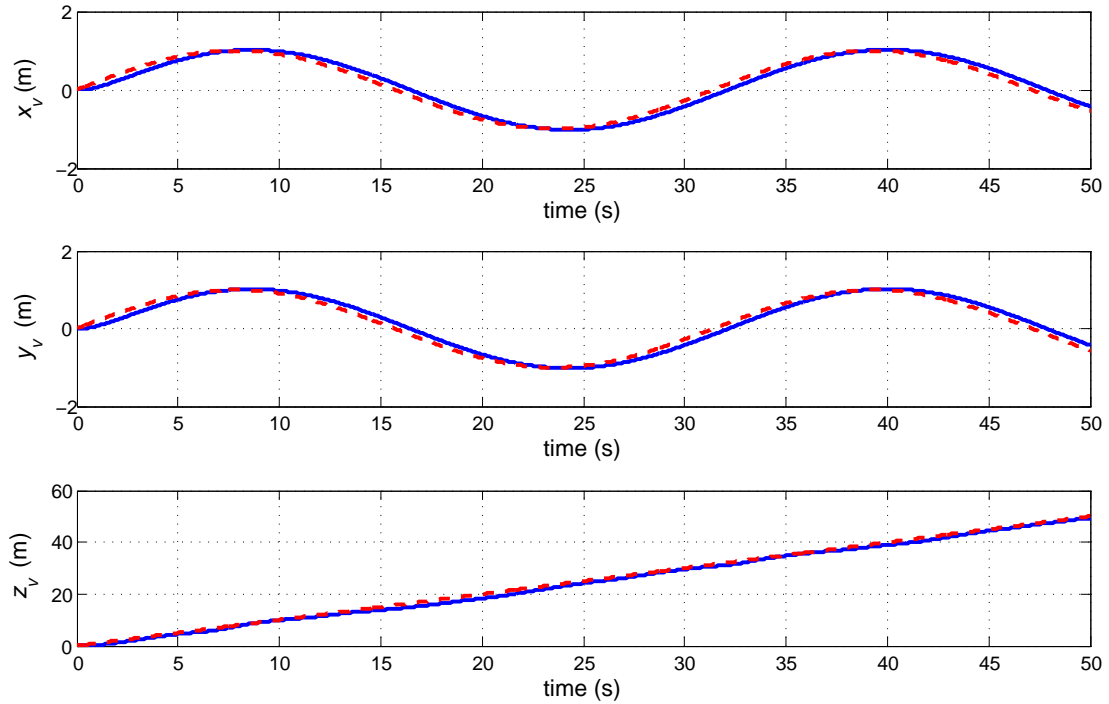


Figure 21. The Cartesian position (solid blue) of the tri-rotor UAV for a rising curved trajectory (dashed red) with input disturbances.

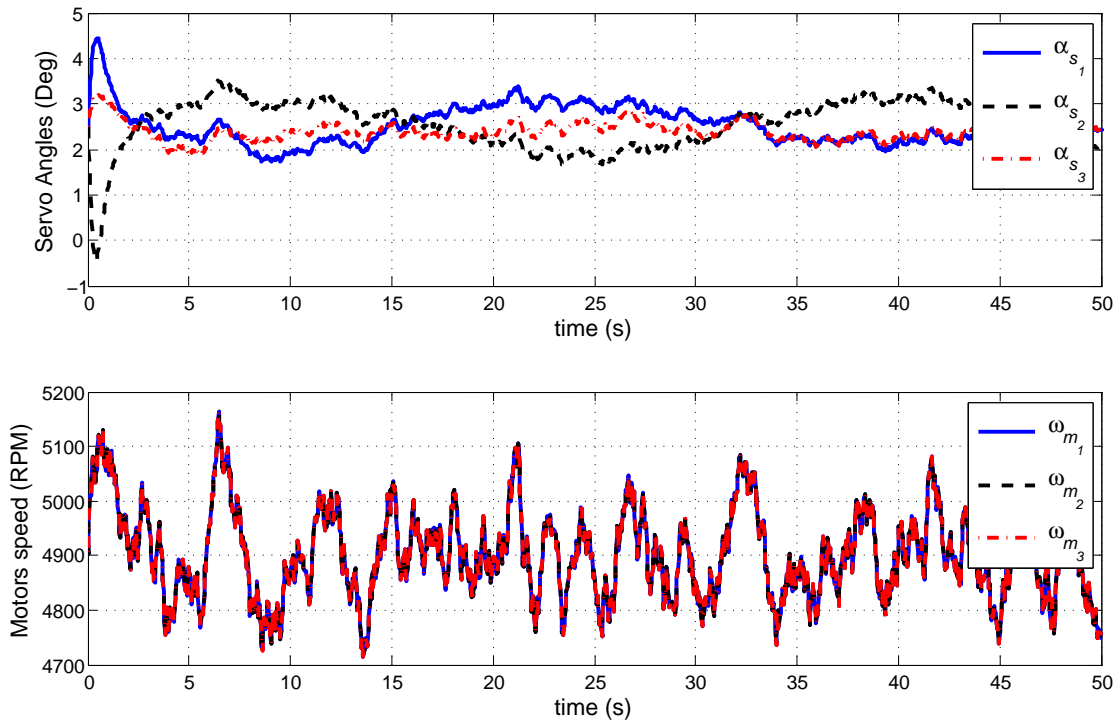


Figure 22. The angles of the servos (top) and the speed of the DC motors (bottom) for a rising curved flight with input disturbances, the tri-rotor UAV.

IV. CASE II: AN OVER-ACTUATED QUADROTOR UAV

This example investigates the proposed control method for an over-actuated system, which is a hinged quadrotor. The system represents the Quansor UAV trainer where the body of the vehicle is attached to a pivot. The construction of the system allows the UAV to move around X , Y and Z axes. Therefore, the system has three outputs, roll (ϕ), pitch (θ) and yaw (ψ), and four inputs u_1 to u_4 which are the input voltage to the rotors. Figure 23 shows a picture of the actual system. The nonlinear model of the system is given by:

$$\begin{bmatrix} \dot{\phi} \\ \dot{\theta} \\ \dot{\psi} \\ \ddot{\phi} \\ \ddot{\theta} \\ \ddot{\psi} \end{bmatrix} = \begin{bmatrix} \frac{\dot{\psi} \tan \theta \cos \phi + \dot{\theta} \sin \phi \tan \theta + \dot{\phi}}{1 - 2 \cos^2 \phi} \\ \dot{\psi} \sin \phi - \dot{\theta} \cos \phi \\ \frac{\dot{\psi} \cos \phi \sec \theta + \dot{\theta} \sin \phi \sec \theta}{1 - 2 \cos^2 \psi} \\ \frac{1}{J_x} (lk_f u_2 - lk_f u_4 + \dot{\psi} J_y \dot{\theta} - \dot{\theta} J_z \dot{\psi}) \\ \frac{1}{J_y} (lk_f u_1 - lk_f u_3 + \dot{\psi} J_x \dot{\phi} - \dot{\phi} J_z \dot{\psi}) \\ \frac{1}{J_z} (k_t u_1 - k_t u_2 + k_t u_3 - k_t u_4 + \dot{\theta} J_x \dot{\phi} - \dot{\phi} J_y \dot{\theta}) \end{bmatrix} \quad (31)$$

Table II lists the parameters of the dynamic model of the quadrotor. The linearised model of the quadrotor around the origin using Taylor series expansion is a second integrator system of four inputs and three outputs as following:

$$P = \begin{bmatrix} 0 & \frac{-lk_f/J_x}{s^2} & 0 & \frac{lk_f/J_x}{s^2} \\ \frac{-lk_f/J_y}{s^2} & 0 & \frac{lk_f/J_y}{s^2} & 0 \\ \frac{-k_t/J_z}{s^2} & \frac{k_t/J_z}{s^2} & \frac{-k_t/J_z}{s^2} & \frac{k_t/J_z}{s^2} \end{bmatrix} \quad (32)$$

As in the previous example, we need to shape the system in order to obtain good frequency response characteristics for the coprime factors N_s and M_s . Figure 24 shows the singular values plot of the original system and the shaped system using a pre and post weights of:

$$W_2 = \begin{bmatrix} 1 & 0 & 0 \\ 0 & 1 & 0 \\ 0 & 0 & 9 \end{bmatrix}, \quad W_1 = \frac{3 \times 10^4 (s+4)^2}{(s+20)^3} \mathbf{I}_{4 \times 4} \quad (33)$$

where the weights W_1 and W_2 are selected using the standard selection criteria discussed in Section II-A.

In this example, the transfer function matrices N_s and M_s have good phase response and therefore no

symbol	definition
l	distance between the gravity center of the quadrotor and each rotor's rotational axis
k_f	force-to-thrust constant of propellers
k_t	torque-to-thrust constant of propellers
J_x	moment of inertial about X (the roll axis)
J_y	moment of inertial about Y axis (the pitch axis)
J_z	moment of inertia about Z axis (the yaw axis)

Table II

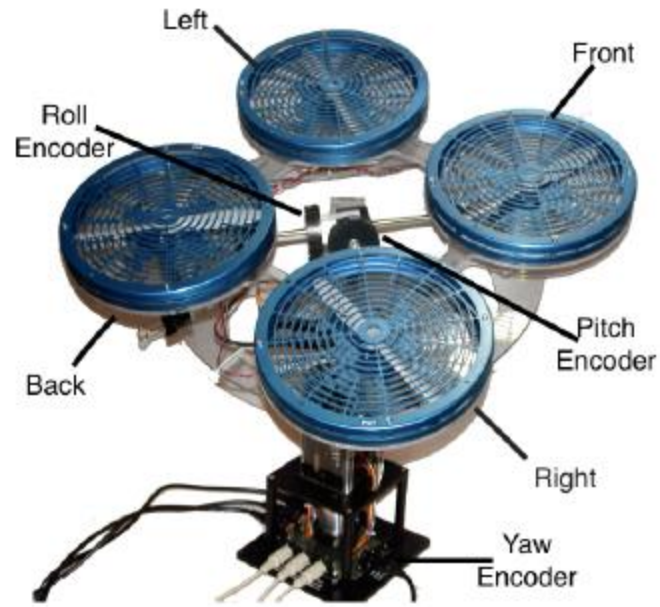


Figure 23. The Quadrotor system. The picture is adopted from [37].

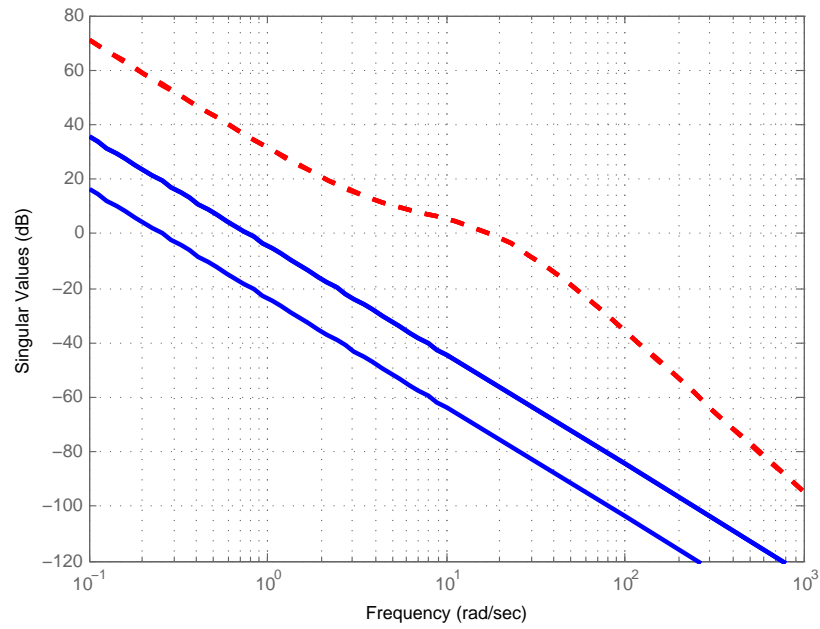


Figure 24. Singular values plot of the linearised system (solid blue) and the shaped system (dashed red) of the quadrotor UAV.

additional phase compensation is required. However, the challenge of this system is that it is not square (3 outputs and 4 inputs). Therefore, in order to construct the Ff/Fb control, a scaling matrix F should be designed to match between the number of the reference channels (3 reference signals) and the required inputs for N_s and M_s (4 inputs). This is due to the fact that N_s and M_s will have specific dimensions (3×4) for N_s and (4×4) for M_s which are related to the size of the original system. In order to achieve this matching, we construct a constant matrix F of suitable dimension (4×3) that gives $FN_s(0) = I$, where $N_s(0)$ is the DC gain of the filter N_s . We then implement the FF/Fb controller by putting $Y = N_s F$ and $X = M_s F$. Figures 25-26 show the singular values plot of the trajectory tracking and the control effort transfer functions of the quadrotor for both cases: the feedback-only control and the Ff/Fb control where both cases have the same feedback controller. These two figures show that the superiority of the Ff/Fb control over feedback-only control where the tracking transfer function of the Ff/Fb control has no overshoot with similar bandwidth to the feedback-only control. The control effort transfer function also shows less actuation in the case of Ff/Fb control. The \mathcal{H}_∞ norm of the closed loop transfer functions confirms these results whereas we have:

$$\begin{aligned} \text{for Ff/Fb: } & \begin{bmatrix} 20\log_{10}(\|T_{ry}\|_\infty) \\ 20\log_{10}(\|T_{ru}\|_\infty) \end{bmatrix} = \begin{bmatrix} 0 \\ 10 \end{bmatrix} \\ \text{and} & \\ \text{for Fb: } & \begin{bmatrix} 20\log_{10}(\|T_{ry}\|_\infty) \\ 20\log_{10}(\|T_{ru}\|_\infty) \end{bmatrix} = \begin{bmatrix} 1.0804 \\ 77.4455 \end{bmatrix} \end{aligned}$$

These values confirm the advantages of Ff/Fb control over feedback-only control where Ff/Fb control has no overshoot and less actuator energy.

Figure 27 shows the frequency response of the closed loop tracking transfer function for the first channel with the Ff/Fb control and the feedback-only control. Figure 28 shows the frequency response of the two actuators (motor 2 and 4) that affect the first output channel, see Eq. (32), with the two control scenarios. For clarity of presentation, we include only information related to the first output channel. The other two output channels have similar properties.

Figure 29(a) shows the time domain simulation of the quadrotor for a square signal trajectory tracking on the pitch and roll channels while keeping the body fixed around z with no yaw rotation. The figure presents good tracking with no overshoot. Figure 29(b) shows the actuator effort of this tracking where all motors work within the physical restriction of $\pm 24\text{V}$ for the input voltage.

To demonstrate the robustness of the proposed Ff/Fb control for this system, we introduce model uncertainty and input disturbances. Similar to the previous example, the model uncertainty is multiplicative of second order as $P_u = P\Delta^2$ with $\Delta = 1 + \frac{a}{s+b}$. Figure 30 shows the performance of the Ff/Fb closed loop system for a model uncertainty of $\Delta = \left(\frac{s+1.721}{s+0.9058}\right)$. Figure 31 demonstrates the performance of the Ff/Fb closed loop system for an input disturbances of $\pm 1\text{V}$. The figures show good performance of the Ff/Fb control under model uncertainty and input disturbances.

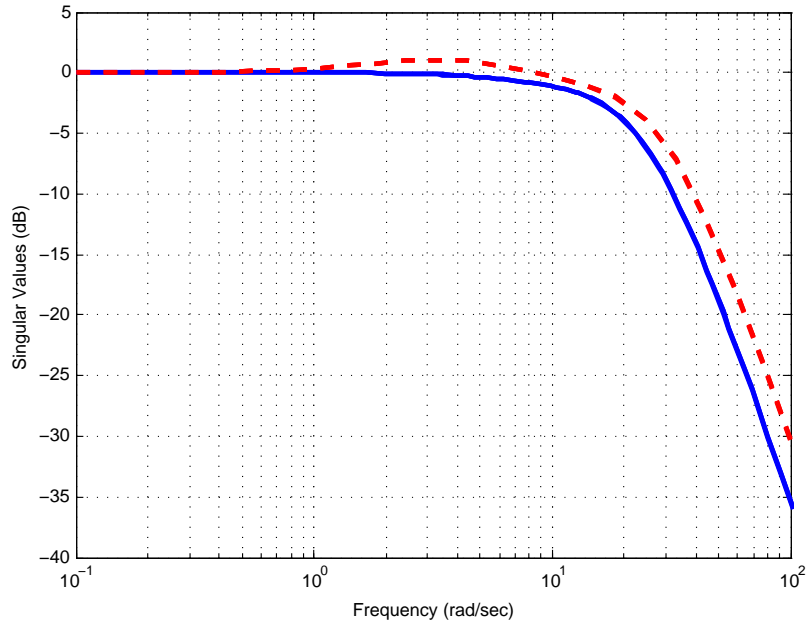


Figure 25. Singular values plot of the tracking transfer function of the quadrotor UAV for two cases: the Ff/Fb control (solid blue) and feedback-only control (dashed red).

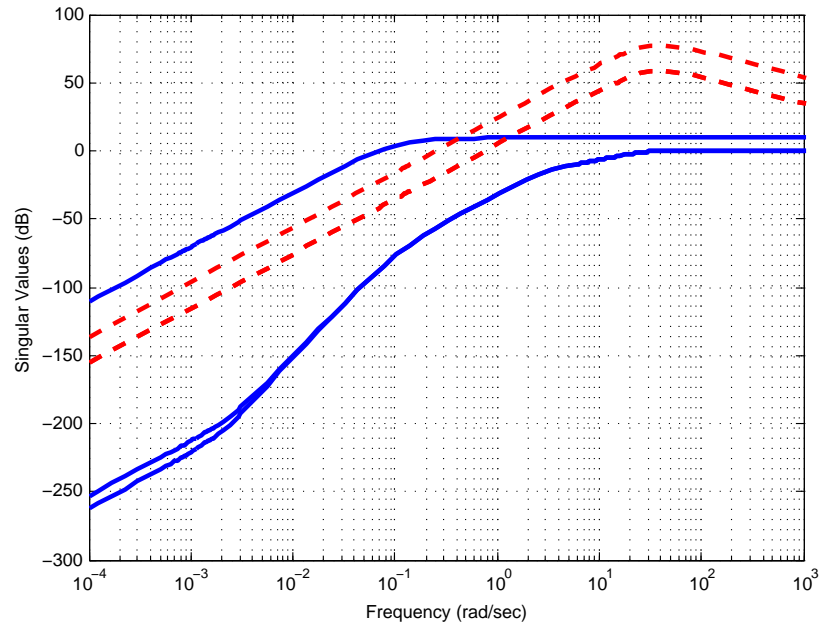


Figure 26. Singular values plot of the control effort transfer function of the quadrotor UAV for two cases: the Ff/Fb control (solid blue) and feedback-only control (dashed red).

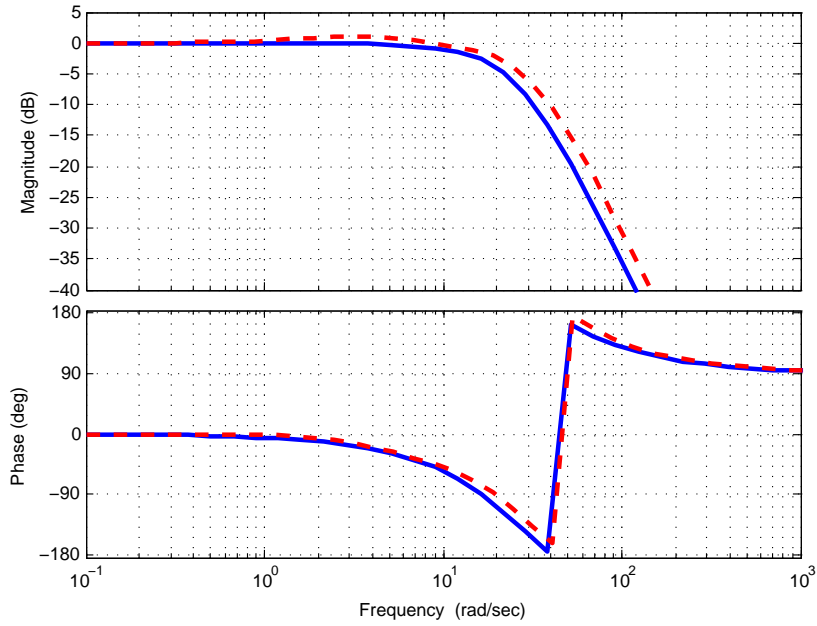


Figure 27. The frequency response of the closed-loop reference-to-output transfer function for the first channel with the Ff/Fb control (solid blue) and the feedback-only control (dashed red).

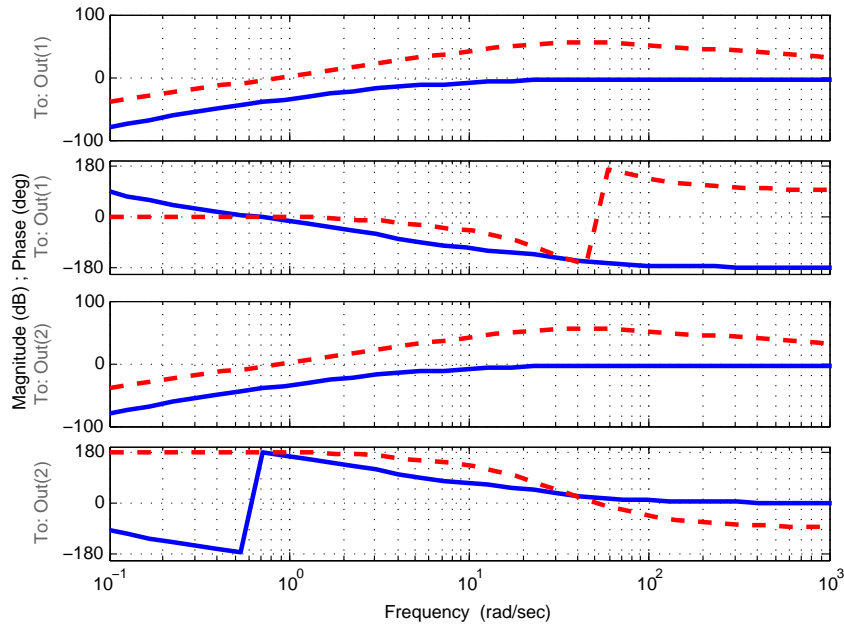
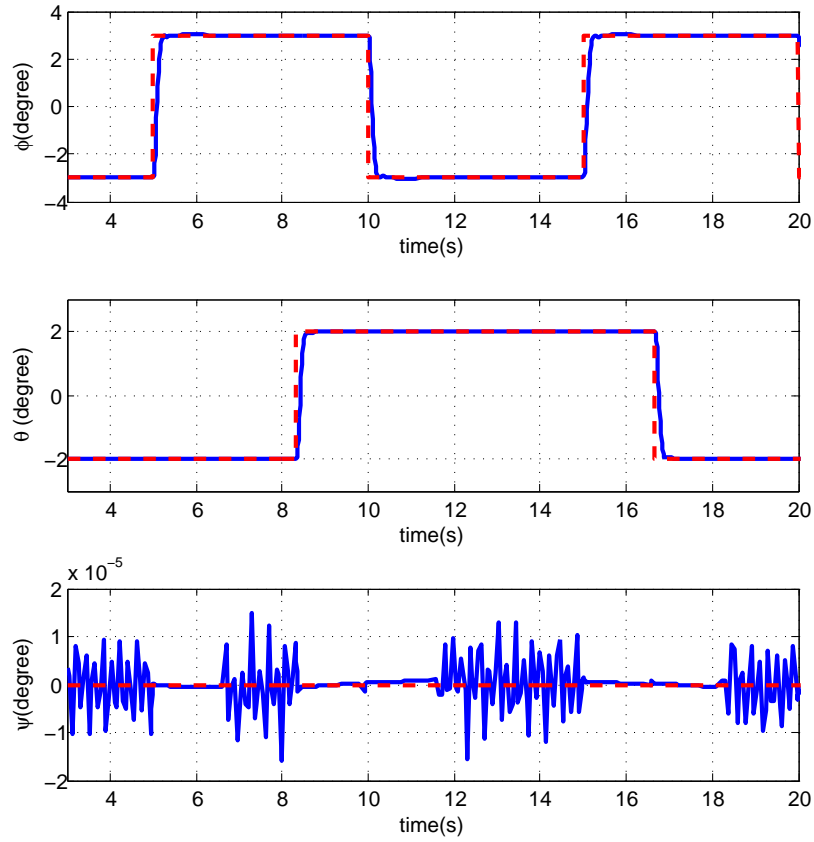
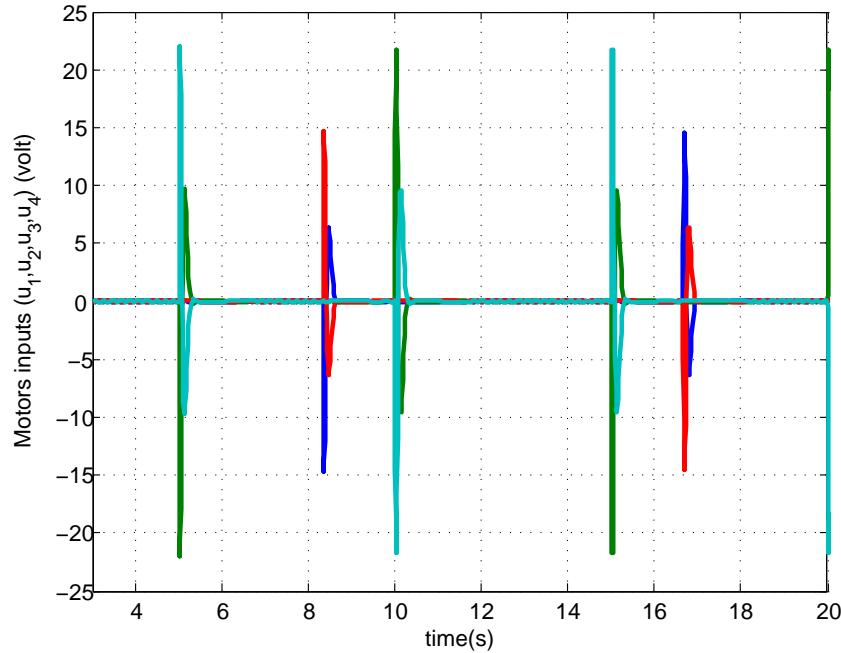


Figure 28. The frequency response of the second and fourth actuators channels of the closed-loop (reference-to-input transfer function) for the case of the Ff/Fb control (solid blue) and the feedback-only control (dashed red).

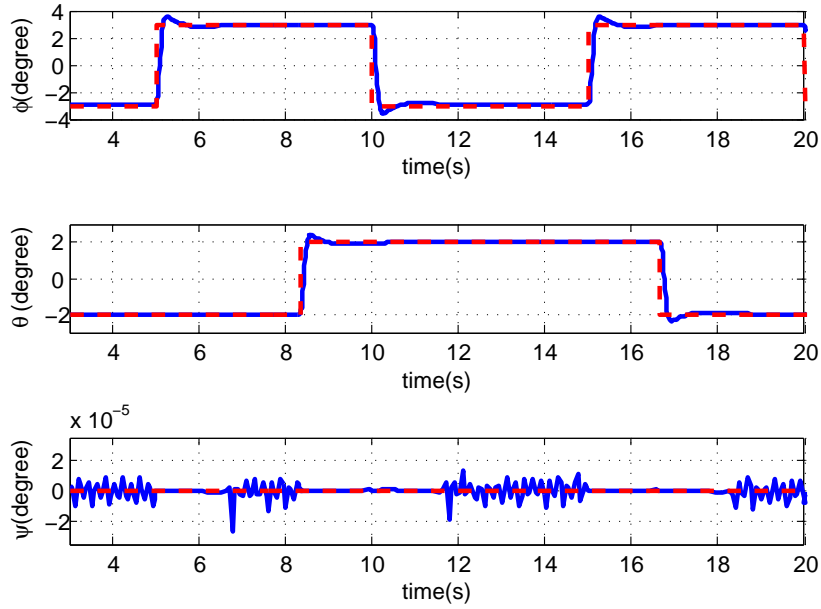


(a) The tracking of the quadrotor UAV (solid blue) for a simultaneous square wave reference signal (dashed red) on pitch channel ϕ and roll channel θ of different frequency and magnitude while keeping the yaw angle ψ at zero.

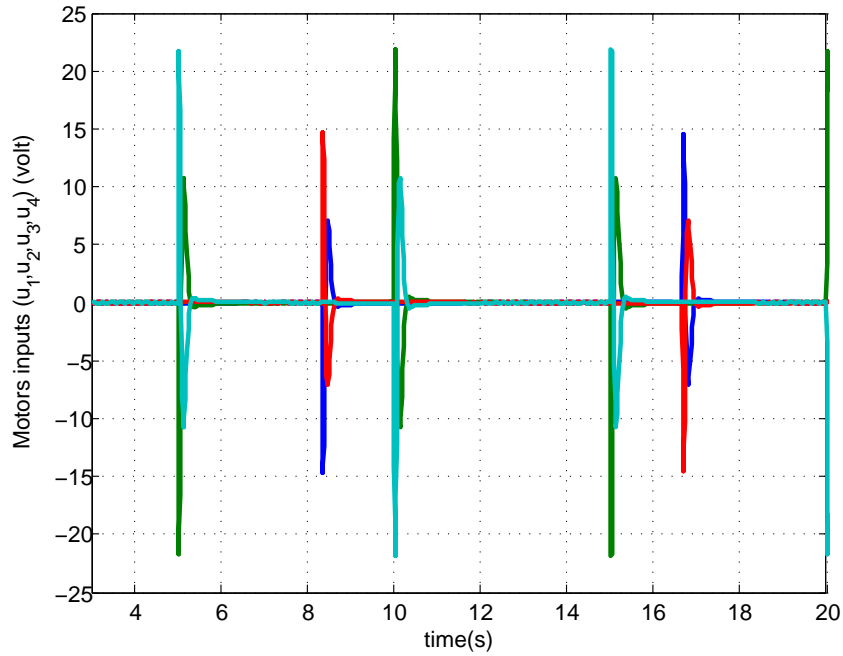


(b) The control effort (motors input voltage) for the attitude tracking.

Figure 29. Time domain simulation of the quadrotor UAV with the Ef/Fb control.

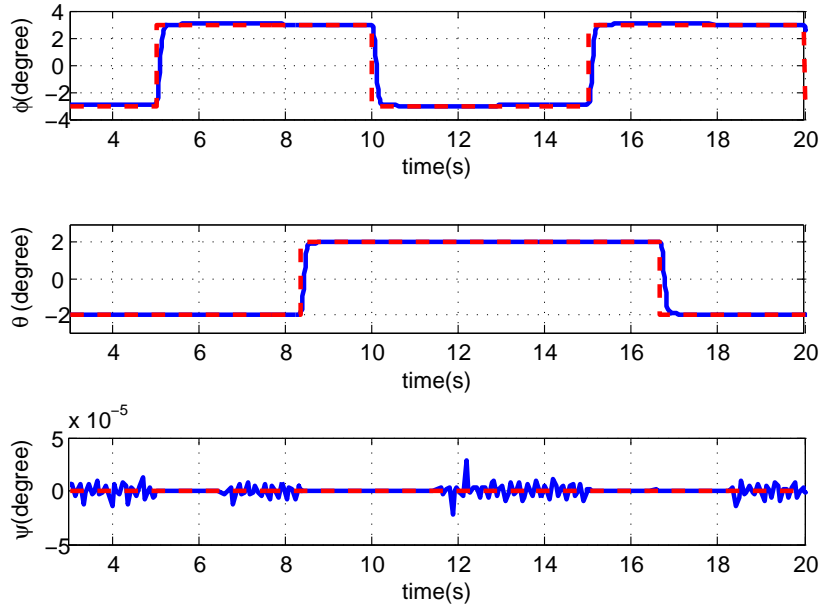


(a) The tracking of the quadrotor UAV (solid blue) for a simultaneous square wave reference signal (dashed red) on pitch channel ϕ and roll channel θ of different frequency and magnitude while keeping the yaw angle ψ at zero.

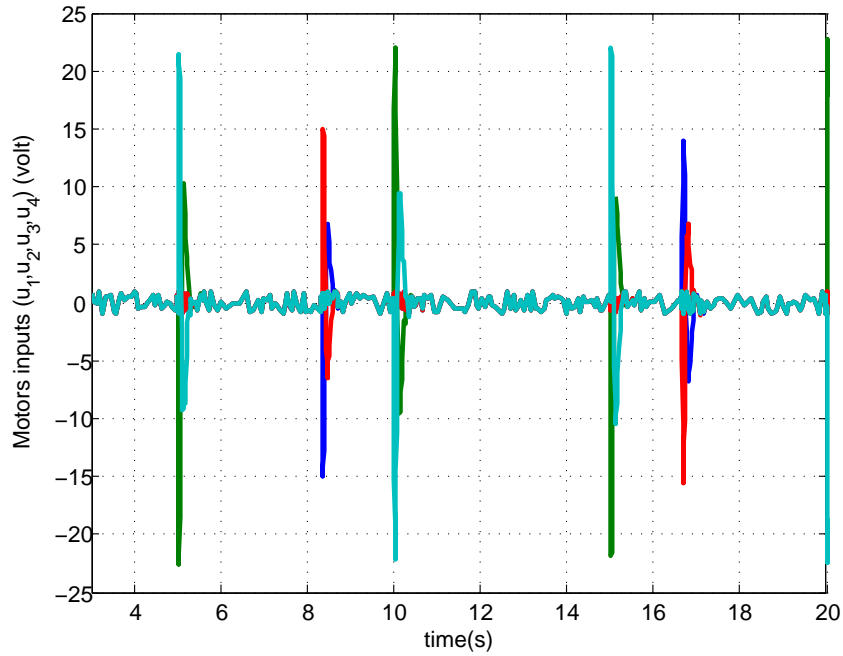


(b) The control effort (motors input voltage) for the attitude tracking.

Figure 30. Time domain simulation of the quadrotor UAV with the Ef/Fb control and model uncertainty.



(a) The tracking of the quadrotor UAV (solid blue) for a simultaneous square wave reference signal (dashed red) on pitch channel ϕ and roll channel θ of different frequency and magnitude while keeping the yaw angle ψ at zero.



(b) The control effort (motors input voltage) for the attitude tracking.

Figure 31. Time domain simulation of the quadrotor UAV with the Ef/Fb control and input disturbances.

V. CONCLUSIONS

This paper proposes a novel feedforward/feedback control algorithm for trajectory tracking and vehicle stabilisation in UAV systems. The design utilises normalised coprime factorisation to construct the reference and feedforward filters in order to eliminate the limitations of the feedback loop. The proposed control system achieves high bandwidth with no overshooting compared with feedback-only control. Results are verified in simulation for a square tri-rotor UAV system and an over-actuated quadrotor trainer.

REFERENCES

- [1] Y. Cui, J. Ren, W. Du, and J. Dai, "UAV target tracking algorithm based on task allocation consensus," *Journal of Systems Engineering and Electronics*, vol. 27, no. 6, pp. 1207–1218, Dec 2016.
- [2] F. Kendoul, "Survey of advances in guidance, navigation, and control of unmanned rotorcraft systems," *Journal of Field Robotics*, vol. 29, no. 2, pp. 315–378, 2012.
- [3] J. Gertler, "U.S. unmanned aerial systems," Congressional Research Service," Technical Report, Jan 2012.
- [4] K. P. Valavanis, Ed., *Advances in Unmanned Aerial Vehicles: State of the Art and the Road to Autonomy*, ser. International Series on Intelligent Systems, Control, and Automation: Science and Engineering. Springer, 2007, vol. 33.
- [5] D. Glade, "Unmanned aerial vehicles: Implications for military operations," Center for Strategy and Technology, Air War College, Air University, Maxwell Air Force Base, Alabama 36112, Technical Report 16, July 2000.
- [6] S. Davies, "UAVs in the firing line," *Engineering & Technology*, vol. 6, no. 8, pp. 34–36, 2011.
- [7] Z. Sarris, "Survey of UAV applications in civil markets," in *Proceedings of The 9th IEEE Mediterranean Conference on Control and Automation*, June 2001.
- [8] M. Okrent, "Civil UAV activity within the framework of European commission research," in *Proceedings of The AIAA 3rd Unmanned Unlimited Technical Conference, Workshop and Exhibit*, Chicago, IL, USA, September 2004, pp. 1–11.
- [9] T. H. Cox, C. J. Nagy, M. A. Skoog, I. A. Somers, and R. Warner, "Civil UAV capability assessment," NASA," Technical Report, Draft Version, December 2004.
- [10] P. Vanblyenburgh, "UAVs: An overview," *Air & Space Europe*, vol. 1, no. 5-6, pp. 43–47, 1999.
- [11] P. Doherty, "Advanced research with autonomous unmanned aerial vehicles," in *Proceedings of The 9th International Conference on The Principles of Knowledge Representation and Reasoning*, Whistler, British Columbia, Canada, June 2004, pp. 731–732.
- [12] S. S. Wegener, S. M. Schoenung, T. Totah, D. Sullivan, J. Frank, F. Enomoto, C. Frost, and C. Theodore, "UAV autonomous operations for airborne science missions," in *Proceedings of The AIAA 3rd "Unmanned Unlimited" Technical Conference, Workshop and Exhibit*, Chicago, Illinois, USA, September 2004, pp. 1–10.
- [13] *Unmanned Aircraft Systems Roadmap 2005-2030*, Office of the Secretary of Defence, Department of Defense, United States of America, August 2005.
- [14] A. Abdessameud and A. Tayebi, "Global trajectory tracking control of VTOL-UAVs without linear velocity measurements," *Automatica*, vol. 46, no. 6, pp. 1053 – 1059, 2010.
- [15] A. Brezoescu, R. Lozano, and P. Castillo, "Lyapunov-based trajectory tracking controller for a fixed-wing unmanned aerial vehicle in the presence of wind," *International Journal of Adaptive Control Signal Processing*, vol. 29, no. 3, pp. 372–384, March 2015.
- [16] A. Aguiar and J. Hespanha, "Trajectory-tracking and path-following of underactuated autonomous vehicles with parametric modeling uncertainty," *IEEE Transactions on Automatic Control*, vol. 52, no. 8, pp. 1362–1379, Aug 2007.
- [17] R. Anderson and D. Milutinovic, "A stochastic approach to dubins vehicle tracking problems," *IEEE Transactions on Automatic Control*, vol. 59, no. 10, pp. 2801–2806, 2014.
- [18] R. Beard, J. Ferrin, and J. Humpherys, "Fixed wing UAV path following in wind with input constraints," *IEEE Transactions on Control Systems Technology*, vol. 22, no. 6, pp. 2103–2117, Nov 2014.
- [19] T. Yamasaki, H. Sakaida, K. Enomoto, H. Takano, and Y. Baba, "Robust trajectory-tracking method for UAV guidance using proportional navigation," in *Control, Automation and Systems, 2007. ICCAS '07. International Conference on*, Oct 2007, pp. 1404–1409.
- [20] Z. Yi, Y. Xiuxia, Z. Hewei, and Z. Weiwei, "Tracking control for UAV trajectory," in *Proceedings of The IEEE Chinese Guidance, Navigation and Control Conference*, Aug 2014, pp. 1889–1894.
- [21] S. Salazar, I. Gonzalez-Hernandez, R. Lopez, and R. Lozano, "Simulation and robust trajectory-tracking for a quadrotor UAV," in *Proceedings of The International Conference on Unmanned Aircraft Systems (ICUAS)*, May 2014, pp. 1167–1174.
- [22] H. Kim, D. Shim, and S. Sastry, "Nonlinear model predictive tracking control for rotorcraft-based unmanned aerial vehicles," in *Proceedings of The American Control Conference*, vol. 5, 2002, pp. 3576–3581 vol.5.

- [23] K. Zhou, J. C. Doyle, and K. Glover, *Robust and optimal control*. Prentice Hall New Jersey, 1996.
- [24] J. Kim, D. Lee, K. Cho, J. Kim, and D. Han, "Two-stage trajectory planning for stable image acquisition of a fixed wing UAV," *IEEE Transactions on Aerospace and Electronic Systems*, vol. 50, no. 3, pp. 2405–2415, July 2014.
- [25] A. Lanzon and I. R. Petersen, "Stability robustness of a feedback interconnection of systems with negative imaginary frequency response," *IEEE Transactions on Automatic Control*, vol. 53, no. 4, pp. 1042–1046, 2008.
- [26] M. Vidyasagar, *Control System Synthesis: A Factorization Approach*, ser. Synthesis Lectures On Control and Mechantronics. Morgan & Claypool, 2011.
- [27] G. Vinnicombe, *Uncertainty and Feedback: \mathcal{H}_∞ loop-shaping and the v -gap metric*. World Scientific, 2001.
- [28] W. H. Press, S. A. Teukolsky, W. T. Vetterling, and B. P. Flannery, *Numerical Recipes: The Art of Scientific Computing*, 3rd ed. Cambridge University Press, 2007.
- [29] M. Kara-Mohamed, W. P. Heath, and A. Lanzon, "Enhanced tracking for nanopositioning systems using feedforward/feedback multivariable control design," *Control Systems Technology, IEEE Transactions on*, vol. 23, no. 3, pp. 1003–1013, May 2015.
- [30] M. Kara-Mohamed and A. Lanzon, "Design and control of novel tri-rotor UAV," in *Proceedings of The UKACC International Conference on Control*, Sept 2012, pp. 304–309.
- [31] M. Kara-Mohamed, "Design and control of UAV systems: A tri-rotor UAV case study," Ph.D. dissertation, School of Electrical and Electronic Engineering, The University of Manchester, UK, September 2012.
- [32] M. Kara-Mohamed and A. Lanzon, "Effect of unmodelled actuator dynamics on feedback linearised systems and a two stage feedback linearisation method," in *Proceedings of the 52nd IEEE Conference on Decision and Control*, Dec 2013, pp. 841–846.
- [33] G. D. Padfield, *Helicopter Flight Dynamics: The Theory and Application of Flying Qualities and Simulation Modeling*, 2nd ed. Wiley-Blackwell Publishing, 2007.
- [34] G. Papageorgiou and K. Glover, "Design, development and control of the HIRM wind tunnel model," in *Proceedings of The 38th IEEE Conference on Decision and Control*, vol. 2, Phoenix, Arizona, USA, December 1999, pp. 1529 – 1537.
- [35] L. Sheng, F. Liang, and L. Jia-lai, "Application of H_∞ control in rudder/flap vector robust control for ship course," in *Proceedings of The International Conference on Mechatronics and Automation, ICMA*, Harbin, China, August 2007, pp. 774–778.
- [36] Y. Jiao, J. Du, X. Wang, and R. Xie, " H_∞ state feedback control for UAV maneuver trajectory tracking," in *Proceedings of The International Conference on Intelligent Control and Information Processing (ICICIP)*, Dalian, China, August 2010, pp. 253 – 257.
- [37] "3 DOF Hover - product information sheet," http://www.quanser.com/Products/3dof_hover, accessed: 2017-03-21.